Atmospheric Environment 360 (2025) 121388

Contents lists available at ScienceDirect

Atmospheric Environment

journal homepage: www.elsevier.com/locate/atmosenv

Unraveling urban nighttime aerosol characteristics and meteorological factors on AOD-PM relationships in East Asia

Jing Li [a], Jiaqi Jin [a], Man Sing Wong [a,b,c,*], Jun Wang [d], Kwon Ho Lee [e], Kai Qin [f], P.W. Chan [g]

[a] Department of Land Surveying and Geo-Informatics, The Hong Kong Polytechnic University, Kowloon, Hong Kong
[b] Research Institute for Sustainable Urban Development, The Hong Kong Polytechnic University, Kowloon, Hong Kong
[c] Research Institute of Land and Space, The Hong Kong Polytechnic University, Kowloon, Hong Kong
[d] Interdisciplinary Graduate Program in Geo-Informatics, The University of Iowa, Iowa City, USA
[e] Department of Atmospheric & Environmental Sciences, Gangneung-Wonju National University, Gangneung, South Korea
[f] School of Environment and Spatial Informatics, China University of Mining and Technology, Jiangsu, China
[g] Hong Kong Observatory, Hong Kong SAR

HIGHLIGHTS

- A comprehensive study of nighttime aerosol characteristics across East Asia.
- Prominent regional differences observed in day-night aerosol variability.
- Consistent vertical distribution of aerosol types between day and night.
- Meteorological factors exhibit notable day-night differences.
- AOD–PM relationships are generally consistent between daytime and nighttime conditions.

ARTICLE INFO

Keywords:
Nighttime aerosol
AERONET
Lunar AOD
Aerosol vertical extinction profile
Vertical aerosol type distribution

ABSTRACT

This study comprehensively investigates nighttime aerosol characteristics across East Asia, addressing a critical gap in current research, as most existing studies focus exclusively on daytime conditions. It systematically examines variations in column-integrated optical properties, vertically resolved extinction profiles, and aerosol-type distributions in six representative regions of East Asia, including Mongolia (MG), Beijing (BJ), Korea (KR), Japan (JP), Hong Kong (HK), and Taiwan (TW). Significant regional differences were identified, with northern regions (MG, BJ, KR, and JP) displaying consistent day-night aerosol optical depth (AOD) and Ångström exponent values. In contrast, southern regions (HK and TW) exhibit pronounced discrepancies. All regions exhibit smoother nighttime extinction profiles than during the daytime. However, northern regions showed sharper vertical decay, while southern regions exhibited secondary peaks attributed to transported smoke aerosols. Additionally, CALIPSO revealed peaks of vertical aerosol distribution at nighttime compared to daytime. Such abnormal phenomenon was then proved to be the more sensitivity of nighttime Lidar signal to upper thin aerosol layers. After removing this bias, the vertical distribution of aerosol types at nighttime is found to be generally consistent with that during the daytime. Meteorological analysis in BJ suggests consistency in AOD-PM relationships between day and night, highlighting temperature as the dominant factor driving seasonal variations in AOD–$PM_{2.5}$ correlations, followed by relative humidity. The findings provide valuable insights into nighttime aerosol characteristics, supporting future research on diurnal aerosol radiative forcing.

1. Introduction

Aerosols are small liquid or solid particles suspended in the atmosphere, broadly categorized into natural and anthropogenic aerosol types (Charlson et al., 1992). Aerosols are intricately linked to the climate system and the hydrologic cycle (Kaufman et al., 2002). They affect Earth's energy budget both directly by reflecting and absorbing sunlight and indirectly by influencing cloud microphysical processes (Li

* Corresponding author. Department of Land Surveying and Geo-Informatics, The Hong Kong Polytechnic University, Kowloon, Hong Kong.
E-mail address: ls.charles@polyu.edu.hk (M.S. Wong).

https://doi.org/10.1016/j.atmosenv.2025.121388
Received 2 April 2025; Received in revised form 27 June 2025; Accepted 30 June 2025
Available online 5 July 2025

et al., 2022). Furthermore, aerosols impact the hydrological cycle by altering cloud cover, cloud properties, and precipitation patterns (Kaufman et al., 2002). In addition to these effects, aerosols significantly contribute to air pollution, driven by secondary aerosol formation, which results in adverse health effects and economic losses (Chen et al., 2018; Huang et al., 2014).

Extensive studies have been conducted on the characterization of aerosols during daytime, while studies on nighttime aerosols are limited despite their critical importance. There is a great need for studying nighttime aerosols. First, the effective radiative forcing (ERF) of aerosol was estimated to be the largest contributor to the overall ERF uncertainty since 1750 (IPCC, 2023). Aerosol optical depth (AOD) is the most critical parameter that determines the radiative forcing, which quantifies the entire light attenuation along the vertical atmospheric column. Existing climate models generally use AOD products from either satellite or ground-based data, such as the Earth Observing System (EOS) Multi-angle imaging spectro-radiometer (MISR), MODerate resolution imaging spectroradiometer (MODIS) satellites, and Aerosol Robotic NETwork (AERONET) (Jia et al., 2021; Khan et al., 2019), which are all daytime AOD products. Second, the growing prominence of nighttime economic activities highlights the need for a better understanding of nighttime aerosols, as their characteristics and impacts are likely distinct from those during the daytime. Meteorological and emission differences between daytime and nighttime significantly influence aerosol properties (Liu and Chan, 2002; Hien et al., 2011). Due to the absence of sunlight at nighttime, the temperature decreases, leading to a lower planetary boundary layer height (PBLH) and reduced vertical convection. This lower boundary layer height traps pollutants, leading to localized air quality degradation, particularly in urban and industrial areas (Su et al., 2018; Tariq and Khan, 2024). Furthermore, the nocturnal dispersion of air pollution emitted from vehicles, industrial processes, and residential heating is suppressed due to the low PBLH and weakened turbulent mixing (Kumar et al., 2021), which further contributes to elevated nighttime aerosol concentrations, and causes serious air quality and health, and even climate issues (Köse et al., 2024). Elevated relative humidity (RH) at night further enhances hygroscopic aerosol growth, significantly altering the properties of aerosols (Jiang et al., 2024). These combined factors imply substantial differences between daytime and nighttime aerosols that remain underexplored.

Previous investigations into day-night differences in AOD have primarily relied on the Cloud-Aerosol Lidar and Infrared Pathfinder Satellite Observations (CALIPSO) satellite data or model simulations. CALIPSO data suggest that nighttime AOD tends to be higher than daytime AOD on both global (Kittaka et al., 2011; Ma et al., 2013), and regional scales, such as eastern China (Gui et al., 2022), and North China Plain (Xu et al., 2019). These studies suggest that higher nighttime AOD can be attributed to lower nighttime temperatures and the hygroscopic growth of aerosols. At the same time, the underestimation of daytime AOD is likely caused by interference from solar radiation. In contrast, Su et al. (2020) reported higher daytime AOD, attributing this phenomenon to the increased anthropogenic emissions during the daytime. Despite these findings, CALIPSO's daytime aerosol products are often underestimated due to challenges in detecting low-level aerosols under the interference of solar radiation (Jiang et al., 2024). Moreover, model simulations generally exhibit lower accuracy than CALIPSO retrievals, further limiting current understanding.

Since 2015, the release of the AERONET lunar aerosol product has provided a more accurate ground-based approach to nighttime aerosol observations, offering new opportunities to study the properties of nighttime aerosols. Several studies have attempted to use AERONET lunar AOD products to characterize nighttime aerosol properties in regions such as Lahore, Pakistan (Tariq et al., 2023), the Indo-Gangetic Plain (Dagestani et al., 2024), and the Beijing-Tianjin-Hebei region (Zhang et al., 2024). However, these studies are geographically localized, and there is a lack of comprehensive investigations into nighttime aerosol properties across East Asia, a region characterized by diverse aerosol types and complex meteorological conditions.

In addition, AOD is often correlated with ground-level particulate matter (PM) concentration, primarily including $PM_{2.5}$ and PM_{10} pollution, which refer to particulate matter with a diameter of 2.5 μm or less and 10 μm or less, respectively. Existing models for AOD-PM relationships can be broadly categorized into scaling and statistical approaches (Ma et al., 2022). While simple linear regression models have been applied, these relationships often break down when aerosols are aloft, necessitating the inclusion of ancillary information such as PBLH and RH (Ma et al., 2022). Advanced regression techniques generally incorporates meteorological variables as supplements due to their potential relationship to aerosol physical and chemical properties (Li et al., 2016). These meteorological variables generally include RH, PBLH, temperature (Temp), wind speed (WS), and wind direction (WD) (Meng et al., 2021; Yao et al., 2019). Existing studies largely focus on daytime aerosols, whereas little research has been conducted on nighttime aerosols. Especially when considering the considerable differences in meteorological parameters between daytime and nighttime. A systematic analysis of how meteorological factors influence the AOD-PM relationship at night is urgently needed.

To address these challenges, this study investigates nighttime aerosol properties across East Asia, focusing on six representative regions: Beijing, Hong Kong, Taiwan, Mongolia, Korea, and Japan. These regions encompass a variety of aerosol types and meteorological influences. The objectives of this study are to comprehensively examine the nighttime aerosol characteristics and daytime-nighttime differences in 1) the aerosol optical properties of the entire atmospheric column, 2) the vertical extinction profiles, 3) the vertical distribution of aerosol types, and 4) the influence of meteorological factors on the AOD-PM relationship, including both fine particles (AOD-$PM_{2.5}$) and coarse particles (AOD-$PM_{10\text{-}2.5}$).

2. Materials

2.1. AERONET data

The AERONET is a globally federated aerosol observation network (Holben et al., 1998). Its daytime aerosol monitoring relies on sun photometers, which provide direct AOD measurements with an uncertainty of approximately 0.01 (Dubovik et al., 2000; Eck et al., 1999). Since 2014, AERONET has expanded its capabilities to include lunar observations using T-CIMEL sun photometers, enabling the production of nighttime AOD datasets. These datasets now include observations at 492 sites. The provisional lunar AOD product is based on the ROLO Irradiance Model, which accounts for extraterrestrial spectral irradiance (Barreto et al., 2013). The most recent updates have been made to the lunar AOD, incorporating the last 5 years of Langleys data, which were used to generate statistically robust ROLO correction factors for each wavelength as a function of lunar phase angle (https://aeronet.gsfc.nasa.gov/, accessed May 14, 2025). The reprocessed dataset of lunar AOD was released in August 2024, having been corrected with the updated empirical bias. AERONET lunar products include AOD and Ångström Exponent (AE) data (Román et al., 2017), which correspond to the aerosol optical properties of the entire atmospheric column. The AOD measures the radiation extinction at a certain wavelength, and it can be used to measure the spectral extinction along with AE. Nighttime measurements are limited to periods of waxing gibbous and full moon phases, as moonlight is significantly fainter than sunlight, allowing coverage of only 50 % of the lunar cycle (Barreto et al., 2013). Additionally, uncertainties in illumination calibration and cloud-screening algorithms result in lower accuracy for lunar AOD measurements compared to daytime sun photometer observations. The accuracy of the lunar and solar measured AOD products are comparable in the AERONET database (Schafer et al., 2024). Version 3 Level 2 data and reprocessed Version 3 Level 1.5 data are used for the solar and lunar AOD products, respectively. Advanced cloud screening quality control

have been introduced in the AOD product of version 3 (Giles et al., 2019). The AERONET AOD at 550 nm was calculated from AOD at 440 nm with an angstrom exponent (440–670 nm) based on the power law (Ångström, 1929). Hereafter, all mentions of AOD refer to AOD at 550 nm. This study utilized AERONET lunar AOD data from six subregions in East Asia, which include 3, 2, 20, 20, 1, and 9 sites in Beijing (BJ), Hong Kong (HK), Japan (JP), Korea (KR), Mongolia (MG), and Taiwan (TW), respectively (Fig. 1).

2.2. CALIPSO extinction profile

The sun-synchronous satellite CALIPSO was launched on April 28, 2006. It has the equator-crossing time of approximately 1:30 p.m. and 1:30 a.m. at local time, with a 16-day repeat cycle. Its primary instrument, the Cloud-Aerosol Lidar with Orthogonal Polarization (CALIOP), is a dual-wavelength polarization lidar designed to capture vertical profiles of attenuated backscatter from a near-nadir-viewing geometry during both daytime and nighttime (Young and Vaughan, 2009). This study utilizes the latest CALIPSO cloud and aerosol products, specifically the Extinction Coefficient at 532 nm from the CALIPSO Lidar Level 2 5-km Aerosol Profile Standard Version 4.51 and the Feature Classification Flags from the CALIPSO Lidar Level 2 Vertical Feature Mask (VFM) Standard Version 4.51, for aerosol profile analysis. The extinction profiles are classified as daytime or nighttime based on the Day/Night Flag and feature a vertical resolution of 0.18 km between altitudes of 20.29 km and 30.01 km, and a vertical resolution of 0.06 km between altitudes of −0.47 km and 20.17 km.

2.3. $PM_{2.5}$ and meteorological data

$PM_{2.5}$ data were obtained from the China National Environmental Monitoring Centre (CNEMC). For this study, $PM_{2.5}$ data from two air quality monitoring stations in Beijing, located near the two AERONET sites (Beijing-CAMS and Beijing_PKU) were used. These data represent particulate matter concentrations near the surface, which are closely linked to aerosols.

Meteorological parameters, including PBLH, RH, Temp, WS and WD were derived from the fifth-generation ECMWF (ERA5) reanalysis datasets (Hersbach et al., 2018). The study used the ERA5 hourly data on pressure levels from 1940 to present (https://cds.climate.copernicus.eu/datasets/reanalysis-era5-pressure-levels?tab=download, accessed on Oct 1st, 2024). Meteorological data at the 1000 hPa pressure level were extracted, with the dataset gridded to a regular latitude-longitude grid of 0.25° (ECMWF, 2024). The meteorological data for the grid centred at 40.0°N and 116.25°E were extracted, which encompass the two AERONET sites in Beijing, and were analyzed. The original wind-related parameters, specifically the U-component (u) and V-component (v) correspond to the eastward and northward winds, respectively. These components were combined to calculate WS and WD using the following equations:

$$WS = \sqrt{u^2 + v^2} \quad (1)$$

$$WD = \mathrm{mod}\left(180 + \frac{180}{\pi}\mathrm{atan}\,2(u, v), 360\right) \quad (2)$$

Note that meteorological wind direction refers to the direction from which the wind is blowing, measured in degrees. It starts at 0° for a north wind (blowing from the north) and increases clockwise: 90° for an east wind, 180° for a south wind, and 270° for a west wind (https://confluence.ecmwf.int/pages/viewpage.action?pageId=133262398, accessed on Jan 5, 2025).

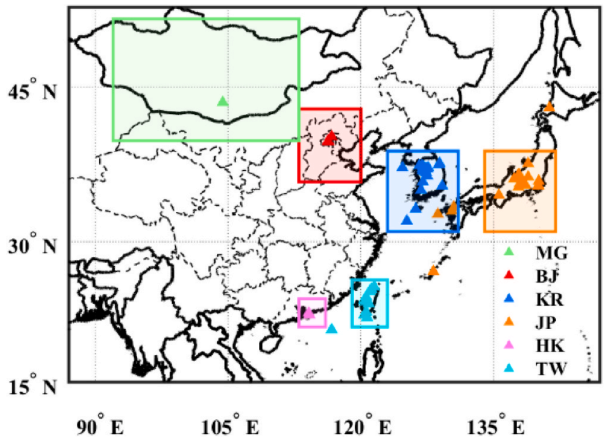

Fig. 1. Study area with the six subregions in East Asia. The triangles denote the locations of AERONET sites, and the rectangles indicate the spatial range for collecting CALIPSO extinction profiles within each of the subregions of MG, BJ, KR, JP, HK, and TW.

3. Method

3.1. Calculation of regional and period averaged vertical extinction profiles

The CALIPSO data for the study areas, spanning 2013 to 2023, were collected and divided into two periods: 2013–2018 and 2019–2023. The Extinction Coefficient and Feature Classification Flags were aligned to the same vertical resolution to produce extinction profiles under strict quality control. The extinction profiles were derived using the extinction coefficient at 532 nm, aided with the cloud-aerosol discrimination (CAD) score. CAD is an indication of the feature type, with values ranging between −100 and 100. Positive CAD scores represent clouds, while negative scores denote aerosols. The absolute value of the CAD score indicates the confidence level of the classification. For this study, only CAD scores ranging from −100 to −20 were used to calculate the extinction profiles, as these correspond to seven aerosol types defined by the VFM products: clean marine, dust, polluted continental, clean continental, smoke, volcanic ash, and sulfate. The mean extinction profiles were calculated for overall aerosols and each specific aerosol type, separately for daytime and nighttime observations. To reduce errors caused by outliers, mean values were computed using the 5th to 95th percentile of the data at each altitude, ensuring robust and reliable estimates for both total and aerosol-specific extinction profiles.

3.2. Analysis of vertical-decomposed aerosol type distribution

Vertical aerosol types of information are provided in the CALIPSO VFM products. Eight aerosol types are involved, including clean marine, dust, polluted continental, clean continental, polluted dust, smoke, volcanic ash, and sulfate. The first six types belong to tropospheric aerosol types, while the latter two belong exclusively to stratospheric aerosol types. Note that tropospheric sulfate is optically ambiguous and typically mixed with other particles, therefore it is typically categorized under broader groups such as polluted continental or smoke (Man-Hae et al., 2018).

For this analysis, only cases with high and medium-confidence levels were considered. The frequency of each aerosol type represents the total number of occurrences during the study period from 2019 to 2023. A preliminary analysis revealed that, compared to daytime, nighttime aerosol types exhibit frequency peaks at higher altitudes. However, this finding contradicts the general understanding that aerosols at nighttime are confined to a lower atmosphere than during the daytime due to the decrease of PBLH. This phenomenon can be attributed to the Lidar's limited ability to detect extremely thin aerosol layers at high altitudes during the daytime due to sunlight interference, resulting in a low

signal-to-noise ratio (SNR). To address this, the study introduces an innovative filtering criterion by excluding aerosol layers with extinction coefficients below 0.1, given that such thin layers generally exhibit weak backscattering signals.

3.3. Analysis of effects of meteorological factors

AOD represents the aerosol loading within the atmospheric column, whereas PM indicates aerosol concentrations near the surface. This study proposes to conduct the analysis by using the correlation coefficient and linear regression slopes, along with the scatterplots. The correlation coefficient quantifies the strength of the relationship between AOD and PM, where a higher coefficient indicates a stronger direct relationship, suggesting AOD can more reliably predict PM values or vice versa. The regression slope reflects the sensitivity of AOD to the changes in PM. A larger slope indicates that minor increases in PM will cause significant increases in AOD. Both the relationships between AOD and fine particulate matter ($PM_{2.5}$), and between AOD and coarse particulate matter (PM_{10}-$PM_{2.5}$) were analyzed, referred to hereafter as AOD-$PM_{2.5}$ and AOD-$PM_{10\text{-}2.5}$, respectively. When constructing the general linear relationship between AOD and PM, it was observed that regression slopes were consistently around 0.01. To enhance the visualization of these relationships, AOD values were scaled by a factor of 100. Consequently, the relationships between AOD*100 and $PM_{2.5}$/$PM_{10\text{-}2.5}$ were constructed, providing a more precise representation of their interaction.

The AOD-PM relationship was first calculated with all available cases from 2015 to 2024. Considering that meteorological effects vary significantly across seasons, the analysis was further categorized into four seasons: spring (March–May: MAM), summer (June–August: JJA), autumn (September–November: SON), and winter (December–February: DJF). A preliminary analysis shows that the correlation of the seasonally decomposed AOD-PM relationship can be significantly improved compared to that derived from all-year cases. Seasonal variations consist of the differences in meteorological conditions. Therefore, this study investigates the impact of meteorological factors' effects on the AOD-PM relationship to better understand its seasonal dependence. Specifically, the AOD-PM relationships were analyzed under different groups classified based on meteorological conditions. Five major meteorological factors involving RH, PBLH, Temp, WS and WD were selected for detailed analysis, as these factors have been shown to influence the AOD-PM relationship significantly (Guo et al., 2017; Li et al., 2016; Zheng et al., 2017).

RH plays a critical role in the relationship between AOD and PM. AOD is measured under ambient (humid) conditions, while PM is determined after heating the air sample, reflecting the dry aerosol mass (Koelemeijer et al., 2006). According to Day and Malm (2001), RH has minimal impact on particle hygroscopic growth when RH $<$ 50 %, a moderate impact when 50 % $\leq$ RH $\leq$ 80 %, and a significant impact when RH $>$ 80 %. Additionally, the day and night histograms of RH reveal a wide distribution spanning from 0 % to 100 %. Based on these observations, RH was categorized into three levels for both daytime and nighttime analyses: low for RH $<$ 50 %, middle for 50 % $\leq$ RH $\leq$ 80 %, and high for RH $>$ 80 %.

The PBLH is closely associated with vertical mixing of aerosols and plays a significant role in the dispersion of pollutants emitted near the surface through various interactions and feedback mechanisms. Su et al. (2018) investigated the relationship between $PM_{2.5}$ concentrations and PBLH and revealing a general negative correlation. Their study found that $PM_{2.5}$ levels decrease sharply as PBLH increases when PBLH is below 500 m. Between 500 m and 1500 m, $PM_{2.5}$ concentrations continue to decline steadily, while beyond 1500 m, $PM_{2.5}$ levels become largely independent of PBLH. Based on these findings, PBLH was categorized into three levels for analysis: low for PBLH $<$500 m, middle for 500 m $\leq$ PBLH $\leq$ 1500m, and high for PBLH $>$1500 m.

Temperature also influences the relationship between AOD and PM and has been considered in previous studies (Hu et al., 2022; Wei et al., 2020). Temperature was classified into three categories for analysis: low for Temp $<$273 K, middle for 273 K $\leq$ Temp $\leq$ 295 K, and high for Temp $>$295 K.

Wind effects, including both wind speed and wind direction, also play crucial roles in the AOD-PM relationship. These factors have been extensively studied in AOD-$PM_{2.5}$ modeling. Wind direction influences the long-range transport of aerosols from surrounding regions. In contrast, wind speed determines whether wind increases aerosol concentrations (e.g., by enhancing mixing) or decreases them (e.g., by dispersing or removing local and transported pollutants) (Zheng et al., 2017). Wind speed was classified into nine levels as suggested by Zheng et al. (2017). The wind direction was classified into two directions, i.e, the north (0-90° and 270-360°) and the south (90-270°). This classification is based on the observation of two peaks in the wind direction histogram and the seasonal Windrose maps.

The region of BJ was selected as a representative case study to examine the impacts of meteorological factors on the AOD-PM relationship. The meteorological effects on the relationship between AOD and PM are driven by similar underlying physical mechanisms. For example, higher relative humidity (RH) increases AOD through hygroscopic growth, even when PM levels remain constant. Higher PBLH enhances convection between the upper and lower atmosphere, leading to a more uniform vertical aerosol distribution. Among the six regions, BJ stands out due to its diverse aerosol sources, including urban emissions, industrial emissions from neighboring Hebei province, dust transported from the upwind Gobi Desert, and oceanic aerosols from the Yellow Sea. Furthermore, BJ experiences distinct seasonal meteorological patterns, making it an ideal location for examining the interplay of meteorological factors and the AOD-PM relationship.

3.4. Estimation of the significance of correlation and correlation difference

To assess the significance of the correlation between AOD and PM, an F-test was conducted at three significance levels α = 0.001, 0.01, and 0.05. To compare the differences in correlation coefficients (r) between daytime and nighttime, Fisher's r-to-z transformation method was applied to evaluate statistical significance (Hawkins, 1989). The correlation coefficients between AOD and PM were initially calculated, and only groups with a significance level higher than 0.05 for both daytime and nighttime were included in the comparison. Subsequently, the r values were transformed to Z value as Equation (3). The final Z statistic for comparing the difference significance was calculated based on Equation (4).

$$z = \frac{1}{2}\ln\left(\frac{1+r}{1-r}\right) \tag{3}$$

$$Z_{observed} = (Z_1 - Z_2) \Big/ \sqrt{\frac{1}{n1-3} + \frac{1}{n2-3}} \tag{4}$$

where n1 and n2 are the sample size of daytime and nighttime, respectively for each group.

4. Results

4.1. Aerosol columnar optical properties

Fig. 2 illustrates the seasonal distribution of aerosol columnar optical properties, i.e. AOD and AE, across six regions during both daytime and nighttime. Higher AOD values indicate greater aerosol loading, while higher AE values signify finer particle sizes. The MG consistently exhibits the lowest AOD during both daytime and nighttime, followed by JP, KR, TW, and HK, whereas BJ maintains the highest AOD throughout the year. The AE values are significantly lower in spring compared to

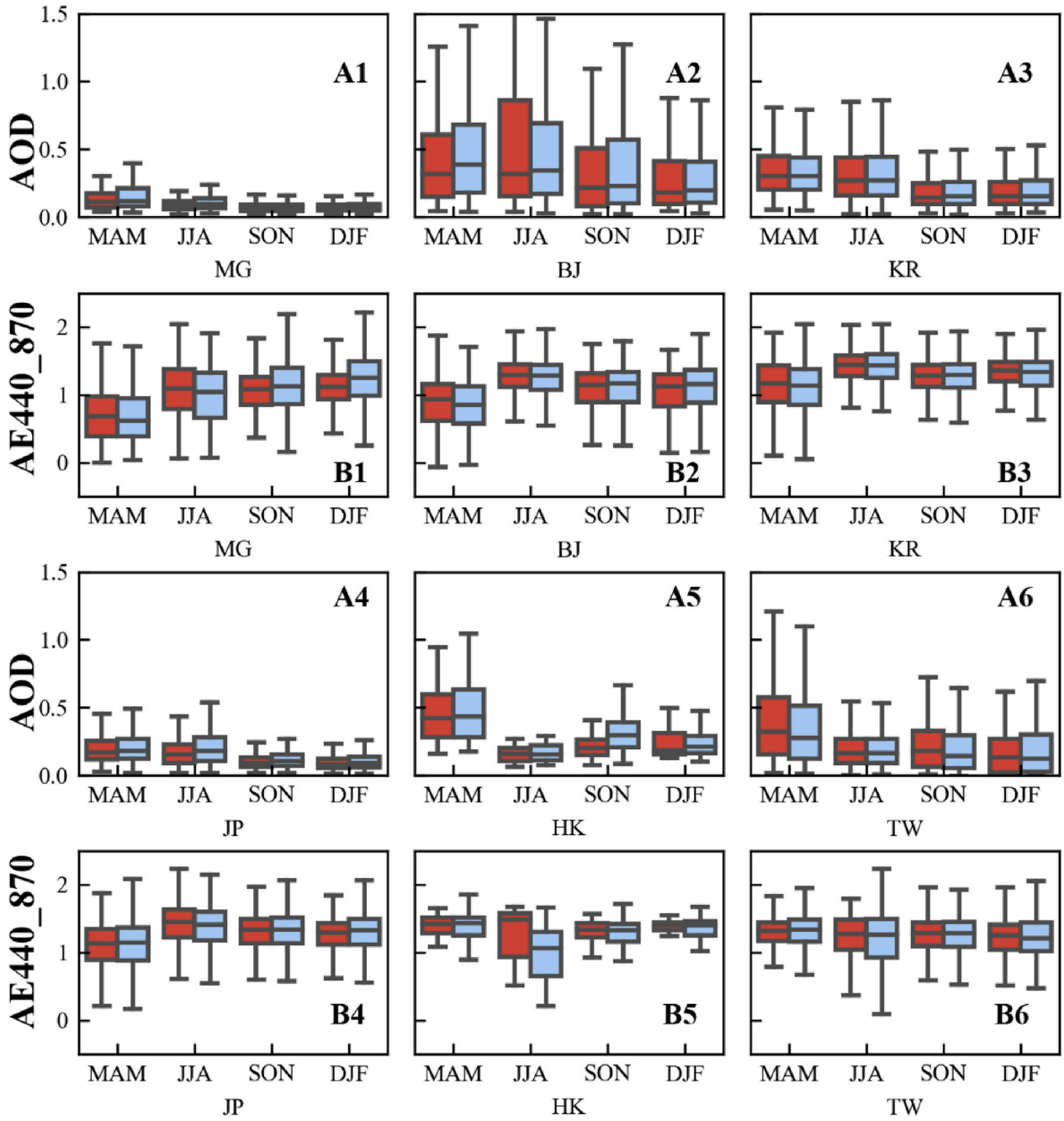

Fig. 2. Seasonal distribution of AOD and AE during spring (MAM), summer (JJA), autumn (SON), and winter (DJF) across the six regions: MG, BJ, KR, JP, HK, and TW. The lines representing the middle, bottom, and top edges of the box represent the median, 25th percentile (Q1), and 75th percentiles, respectively, of AOD and AE values. The height of the box is the interquartile range (IQR) = Q3-Q1. The lowest and highest lines denote the Q1-1.5*IQR, and Q3+1.5*IQR of AOD and AE values.

other seasons in the four northern regions (MG, BJ, KR, and JP), likely due to the influence of dust aerosols. In contrast, AE values for HK and TW remain relatively higher, as these regions are less affected by dust aerosols. By comparing the nighttime and daytime AOD and AE, general consistencies were found for the four northern regions. However, HK and TW display pronounced differences in both AOD and AE, which can be attributed to variations in relative humidity (RH) and emissions. The northern regions typically experience lower RH, while the southern regions, including HK and TW, exhibit higher RH. Day and Malm (2001) found that the hygroscopic growth of aerosols does not increase linearly with RH. The hygroscopic growth is minimal when RH $<$ 50 %, and it grows slowly from around 50 %–80 %, while growth sharply when RH exceeds 80 %. Therefore, although RH increases at nighttime in the four northern regions, it may be insufficient to cause significant hygroscopic growth of aerosols. Instead, in HK and TW, especially in summer, RH often exceeds 80 % at nighttime, leading to noticeable hygroscopic

growth, as shown in Fig. 2 (B5 and B6). In addition to hygroscopic growth, high humidity can also lead to higher cloud coverage, thereby increasing the AOT level (Eck et al., 2018). Notably, TW consistently shows lower nighttime AOD values compared to those in daytime across all four seasons (Fig. 2 A6), suggesting reduced local emissions at night. In contrast, average nighttime AOD values in HK are generally higher than those during the daytime across the seasons, especially noticeable in autumn (Fig. 2 A5). This phenomenon could be attributed to two factors. First, nighttime land breezes may transport pollutants from the nearby Greater Bay Area, which typically experiences higher pollution levels than HK. Second, the stably stratified flow over the region could contribute to pollutant accumulation, as highlighted by Liu and Chan (2002).

Fig. 3 illustrates the relationship between AE and AOD at nighttime. Fig. 3A1 to A4 show that high AOD are generally associated with low AE over the region of MG, suggesting that high AOD in this area is primarily caused by aerosols with larger particle sizes. This is likely due to the frequent occurrence of dust aerosols over Mongolia. Additionally, in the BJ, KR, JP, and TW regions, high AOD is generally associated with large AE values during summer, autumn, and winter, indicating that fine particles contribute significantly to high AOD at nighttime in these regions and seasons. For example, Fig. 3 reveals that high AOD values ($>$1.0) correspond to large AE values of approximately 1.5 in summer, autumn, and winter over BJ. Similarly, Fig. 3 C2 to C4 show that in KR, high AOD values ($>$1.0) are associated with AE values of 1.5, 1.4, and 1.2 in summer, autumn, and winter, respectively. The region of JP exhibits a similar pattern to KR, as shown in Fig. 3 D2 to D4. TW demonstrates a slightly different trend, where high AOD values ($>$1.0) correspond to AE values of 1.4, 1.4, 1.2, and 1.1 in spring, summer, autumn, and winter, respectively (Fig. 3 F2 to F4). HK shares some similarities with TW, but due to the limited number of nighttime cases, the observed patterns are less pronounced (Fig. 3E2 to E4). The relationship between AE and AOD at daytime is illustrated in Fig. A1, showing a similar pattern to that observed at nighttime. High AOD values are generally associated with high AE in regions of BJ, KR, JP, HK, and TW, indicating that fine-mode particles predominantly contribute to high AOD in these regions. In contrast, high AOD values in MG are generally accompanied by low AE values, suggesting that coarse-mode particles are the primary contributors to the elevated AOD in this region.

4.2. Vertical extinction profiles

To investigate the daytime and nighttime aerosol characteristics along the vertical direction, CALIPSO extinction profiles and aerosol type classification data from 2013 to 2023 were analyzed. The data were divided into two periods: 2013–2018 and 2019–2023, using 2019, the year marking the onset of COVID-19, as a division point.

Fig. 4 presents the average extinction profiles for both day and night across six regions during the two periods. The number of cases used to do the average is displayed in Fig. A2. More cases were found at lower altitudes compared to those at higher altitudes, which partly explains the large fluctuations observed at higher altitudes. Compared to 2013–2018, the rate of extinction at lower levels over BJ decreased significantly at both daytime and nighttime in the period of 2019–2023, suggesting improved air quality in recent years due to China's air quality control policy (Zheng et al., 2024). Daytime extinction over MG has markedly increased, while its nighttime extinction remains similar between the two periods. This suggests that the increased extinction is likely due to more frequent dust events in recent years, as dust typically occurs during the daytime, resulting from stronger winds. For HK, TW, KR, and JP, the extinction profiles for both daytime and nighttime are relatively consistent, with only minor differences.

Compared to the extinction profiles during the daytime, the nighttime extinction profiles exhibit sharper exponential decay, indicating a lower PBLH at nighttime (Fig. 4). This suggests that nighttime aerosols are mostly confined to the lower atmosphere. In contrast, daytime aerosols exhibit more fluctuations along the vertical direction. The extinction profiles for BJ, KR, and JP exhibit smooth exponential decay, whereas notable fluctuations are observed in the profiles for MG, HK, and TW. Over MG, a second extinction peak appears around 1 km for both time periods, likely corresponding to dust aerosol layers. Additionally, it is noteworthy that the extinction profiles for HK and TW, both during the day and at night, deviate from the typical exponential decay pattern. Instead, secondary extinction peaks are observed at altitudes approximately 2–4 km. These peaks are likely to be caused by the transported smoke aerosols, as supported by Fig. 5, which shows a high frequency of smoke at this elevation range. The smoke aerosols are possibly transported from southeast Asia (Zeng et al., 2023). Besides, several abnormal extinction peaks were identified at altitudes higher than 5 km over HK and TW, which are likely due to misclassified cirrus. As cirrus clouds exhibit depolarization ratios similar to those of dust aerosols, they may be erroneously identified as dust at high altitudes (Man-Hae et al., 2018).

The day-night difference in extinction profiles at lower altitudes ($<$2 km) can be explained by local emissions and meteorological factors. The local emissions are generally higher during the daytime due to more frequent human activities and transportation in urban areas. Therefore, considering emissions alone, aerosol extinction should generally be higher during the daytime than at nighttime. However, it was also commonly found that high RH at nighttime could cause a hygroscopic growth of aerosols and more cloud cover, which in turn enhances the extinction coefficient (Jiang et al., 2024). This creates a balance between emission-driven and meteorological-driven effects on extinction. The averaged extinction profiles at 2 km are displayed in Fig. A3, which shows that all daytime extinction profiles are significantly greater than those at nighttime, with a p-value less than 0.01. This could be attributed to the higher emissions at daytime. Notably, there are nighttime extinction peaks over HK at around 300 m, where the nighttime extinction is even greater than the daytime. Such a peak is possibly caused by meteorological factors. For regions of KR, JP, and TW, their extinction coefficients are relatively lower compared to the other regions, displaying extinction less than 0.1 per km.

4.3. Vertical aerosol type distribution

Fig. 5 presents the seasonal vertical frequency distribution of eight aerosol types, including clean marine, dust, polluted continental, clean continental, polluted dust, smoke, volcanic ash, and sulfate. Note that volcanic ash, and sulfate belong to stratospheric aerosol types as in the CALIPSO VFM product. Therefore, it was found that the two aerosol types are rarely observed, as only the range from 0 to 10 km is displayed. Besides, the polluted dust type is generally the anthropogenic emissions from local or regional areas, while the dust type is the natural mineral dust from desert areas (Chen et al., 2025). The six regions can be grouped into three categories, which show similar seasonal vertical frequency distribution patterns. MG and BJ are dominated by two aerosol types across all seasons, i.e. polluted dust and dust. KR and JP are only dominated by dust in spring, while clean marine is the dominant one in the other seasons. HK and TW are dominated by smoke only in spring, while they are dominated by clean marine in the other seasons. The dominance of dust in the four northern regions (MG, BJ, KR, and JP) could be attributed to frequent dust activities in spring in Northeast Asia (Li et al., 2024). Notably, Fig. 5 identifies polluted dust aerosol in spring and winter in the four northern regions. Such phenomenon could be explained by Tao et al. (2022), which highlights unnoticeable but frequent dust plumes as the dominant sources of prevailing dust particles over East Asia, which appear most frequently in spring and followed by winter.

It was noticed that more aerosols appear at higher altitudes at nighttime than daytime, which is contrary to the understanding that low PBLH confines the aerosol in the lower layers at nighttime. It was thus

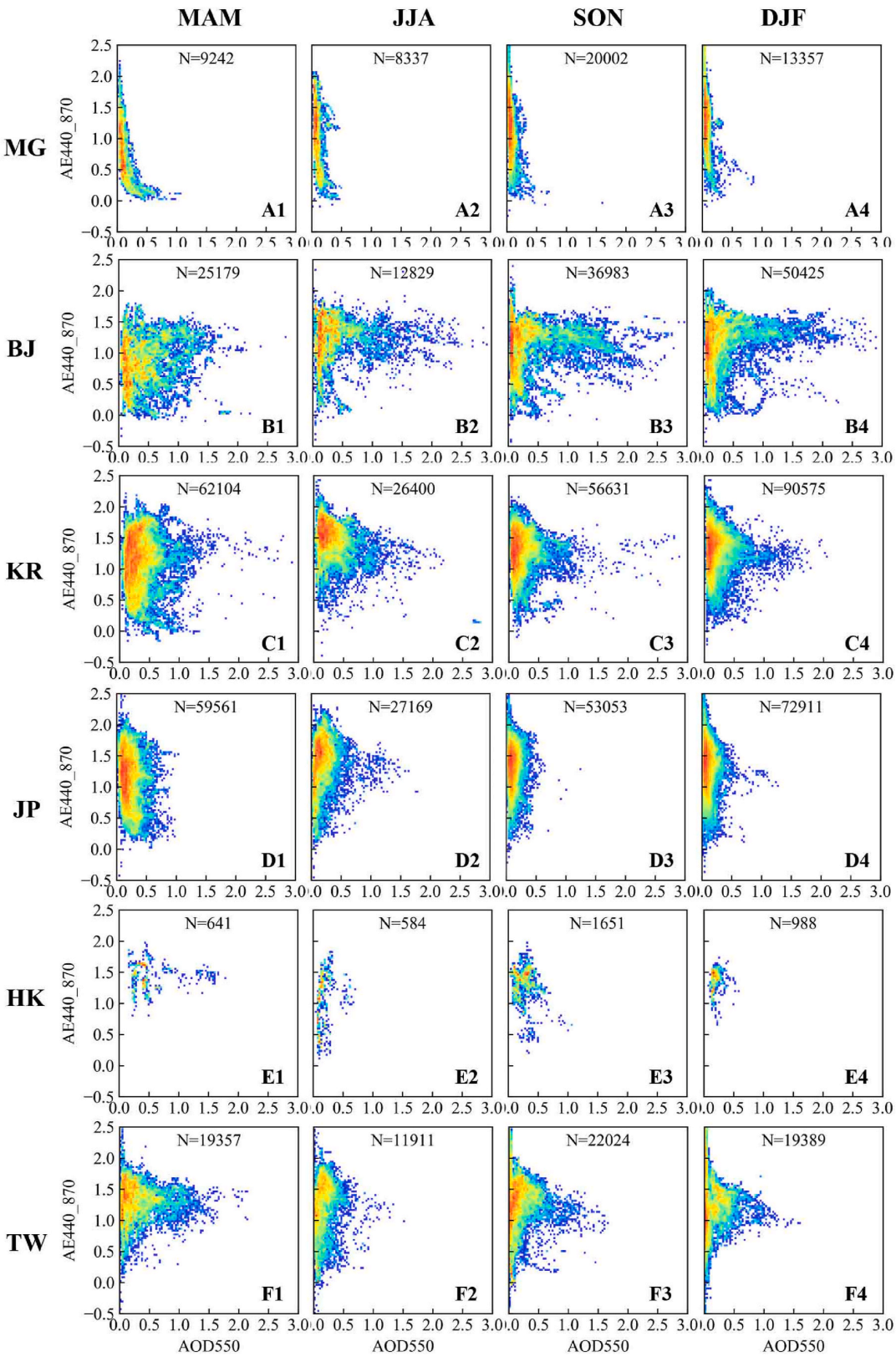

Fig. 3. Scatterplots of the relationship between nighttime AE and AOD during spring (MAM), summer (JJA), autumn (SON), and winter (DJF) across the six regions: MG, BJ, KR, JP, HK, and TW.

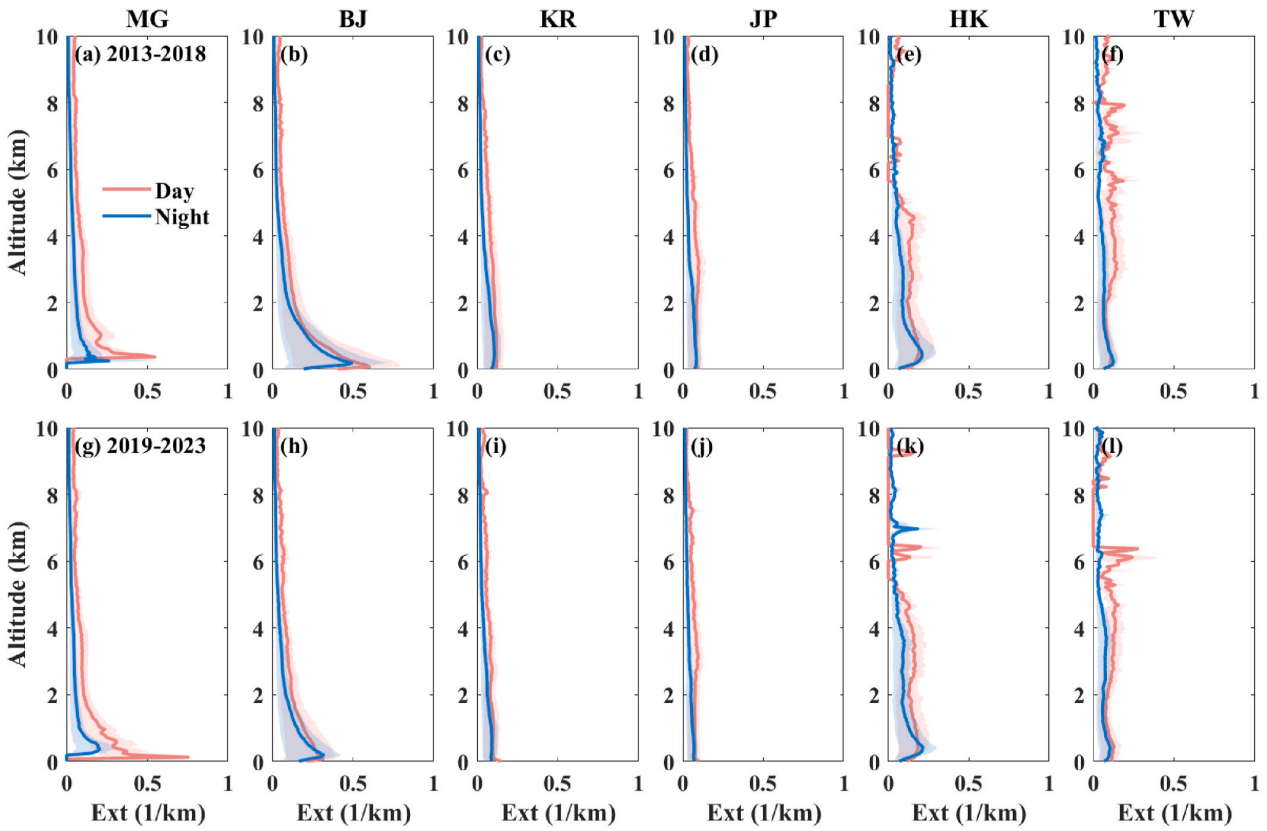

Fig. 4. Averaged extinction profiles from 0 to 10 km for the two periods: 2013–2018 and 2019–2023, across the regions MG (a and g), BJ (b and h), KR (c and j), JP (d and j), HK (e and k), and TW (f and l).

assumed that such nighttime biases are due to the higher sensitivity of the Lidar signal at night. Therefore, the vertical frequency distributions of aerosol types were further decomposed to the thick and thin aerosol layer based on an extinction threshold of 0.1 in Figure A4 and Figure A5, respectively. After decomposition, Fig. A4 shows the consistency of vertical frequency distribution between daytime and nighttime for all aerosol types, while Fig. A5 exhibits even larger nighttime biases. The results support the assumption that the nighttime biases are caused by nighttime Lidar signals' sensitivity to thin layers. Consequently, it can be concluded that the aerosol types should be similar between daytime and nighttime.

To investigate the extinction magnitude of each aerosol type and its variations along the vertical direction, the extinction profiles for both day and night were averaged across the seven aerosol types for the two periods (Fig. 6). Cases with extinctions greater than 0.5 and at altitudes higher than 5 km are removed because they are likely to be misclassified cirrus clouds. Fig. 6 illustrates the general consistency in extinction profiles across the two periods. Among the aerosol types, smoke exhibits the highest extinction magnitude, followed by polluted continental, polluted dust and dust types, while clean continental and clean marine aerosols show minimal extinction. Volcanic ash and sulfate aerosols are typically classified in the stratosphere aerosol types, and thus, they show at high altitudes.

4.4. Impacts of meteorological factors on the relationship between AOD and PM

4.4.1. Diurnal and seasonal patterns of the meteorological factors

Fig. 7 depicts histograms and seasonal diurnal variations of the five meteorological factors involving PBLH, RH, Temp, WS, and WD in the region of BJ. The most significant day-night difference is observed for PBLH, which is up to 10 times higher during the day than at night (Fig. 7a). Daytime PBLH varies notably between seasons, with the highest values in spring, followed by summer, and the lowest in winter and autumn, which is consistent with the results of Zheng et al. (2017). The high PBLH in spring may be associated with the strongest near-surface wind speed, while high PBLH in summer could be associated with solar radiation (Zheng et al., 2017). At nighttime, seasonal differences in PBLH are minimal (Fig. 7b). It should be noted that the estimated diurnal PBLH differences could be exaggerated than the actual conditions, as ERA5 reanalysis data tend to slightly overestimate the PBLH during the daytime while underestimating it at nighttime, as revealed in Zhang et al. (2020) and Peng et al. (2023). These studies also suggest that typical diurnal variations in PBLH differences are approximately two-to three-fold. Nevertheless, ERA5 reanalysis data are considered suitable for this study, as they reliably capture the diurnal pattern and have been widely used in building the relationship between AOD and $PM_{2.5}$ (Ma et al., 2022; Song et al., 2022). RH is generally higher at night, with more occurrences of RH exceeding 50 % compared to daytime (Fig. 7c). Seasonally, RH peaks in summer, followed by autumn, spring, and winter (Fig. 7d). Temp shows the smallest day-night variation, with daytime temperatures 2–4 K higher than nighttime values (Fig. 7e). Seasonal differences are much more pronounced, with the highest temperatures in summer, followed by spring and autumn, and the lowest in winter (Fig. 7f). WD exhibits comparable day-night and seasonal differences, with variations of about 1–2 m/s (Fig. 7g and h). Winter and spring exhibit similarly strong winds, with slightly higher daytime wind speeds (WS) in spring and higher nighttime WS in winter, while summer has the weakest winds (Fig. 7h).

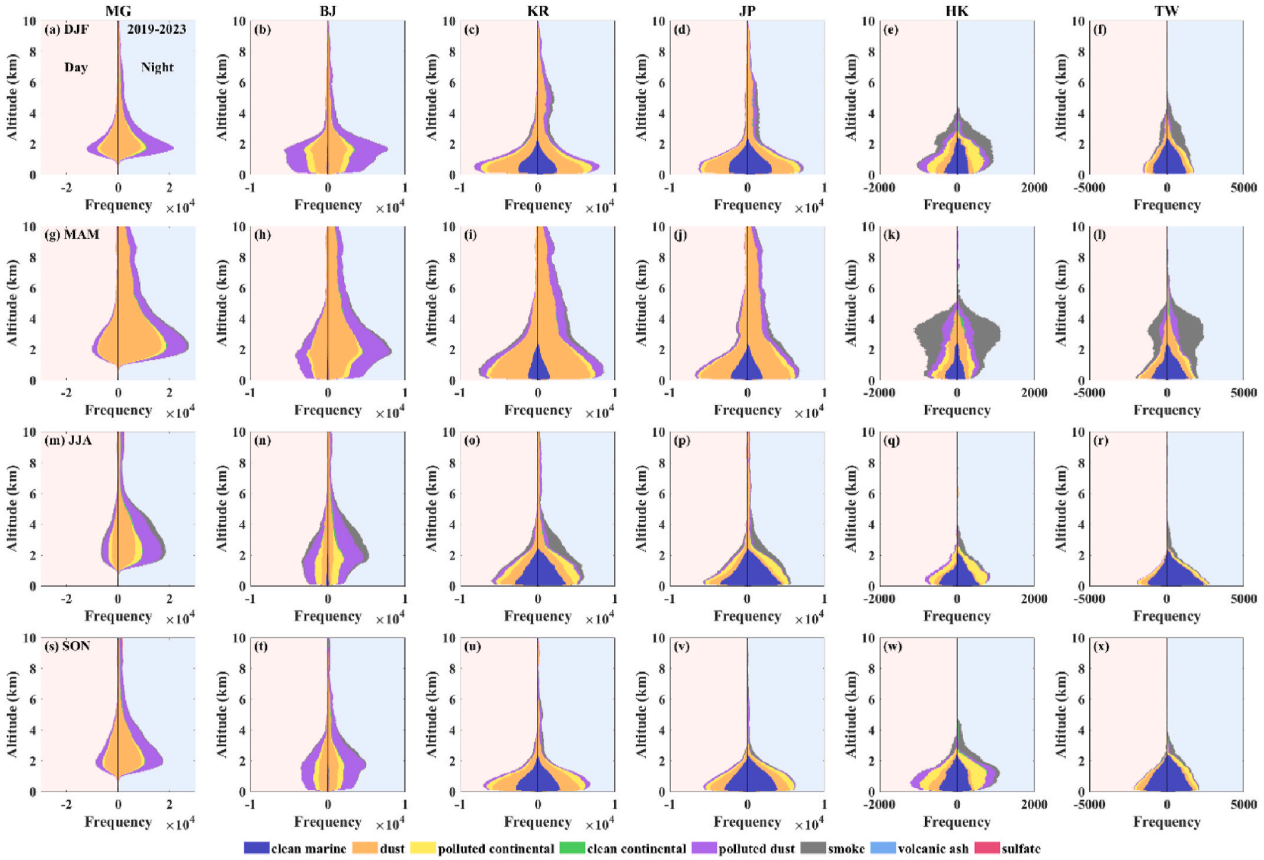

Fig. 5. Seasonal vertical frequency distribution of aerosol types across the regions of MG, BJ, KR, JP, HK, and TW during the period of 2019–2023.

4.4.2. Overall and seasonal AOD-PM relationship

Fig. 8 presents scatterplots of AOD versus PM for overall cases from 2015 to 2024. Correlation coefficients between AOD and PM ($PM_{2.5}$/$PM_{10\text{-}2.5}$) are slightly higher during daytime (0.630/0.168) than at nighttime (0.623/0.142), though the differences are statistically insignificant. The slopes at daytime are also slightly higher than those at nighttime, indicating AOD is more sensitive to the increase of PM.

Fig. 9 shows seasonal scatterplots of AOD versus $PM_{2.5}$, where correlation coefficients improve across all four seasons for both daytime (0.7325, 0.700, 0.702, 0.695) and nighttime (0.669, 0.681, 0.723, 0.642) periods, compared to the overall cases. However, such seasonal improvements are minimal for AOD-$PM_{10\text{-}2.5}$ relationships Fig. 10. The seasonal differences on the AOD-PM relationship are mainly influenced by the meteorological factors including PBLH, RH, temperature, and wind. The following section further explores the impacts of these meteorological factors on the AOD-PM relationship.

4.4.3. The AOD-PM relationship under grouped meteorological factors

PBLH affects the AOD-PM relationship primarily by either confining aerosols within a shallow PBLH or allowing more space for aerosol mixing under a deeper PBLH. For both daytime and nighttime, the AOD-$PM_{2.5}$ correlation generally increases with deeper PBLH (Fig. 11). Specifically, the correlation improves from 0.5988 to 0.724 during the day and from 0.608 to 0.645 at night as PBLH increases from low to high. This trend suggests that deeper PBLH enhances the correlation between AOD and $PM_{2.5}$, likely due to a deeper PBLH promoting more homogeneous aerosol mixing. As a result, the extinction coefficient becomes more vertically uniform, aligning the relationship between AOD and $PM_{2.5}$ closer to the equation AOD = a*$PM_{2.5}$*PBLH. The slope of AOD-$PM_{2.5}$ also increases with PBLH during the day, from low (0.73) to high (0.96). However, the nighttime slope peaks under the middle PBLH condition (Fig. 11e). The low slope observed at high PBLH at nighttime may be attributed to the limited sample size in this category (only 66 samples). The AOD-$PM_{10\text{-}2.5}$ relationship exhibits similar correlation trends, with higher PBLH corresponding to increased correlations during both daytime and nighttime. Since nighttime PBLH tends to skew toward lower values, an alternative set of thresholds (T2) was introduced to ensure statistical significance: PBLH<100, middle for 100 m < PBLH <200 m, and high for PBLH >200 m. This adjustment provided sufficient samples in the high PBLH group (Fig. A6). Under these thresholds, both correlation coefficients and slopes for the AOD-$PM_{2.5}$ relationship increased with PBLH, with correlation coefficients rising from 0.607 to 0.721 and slopes increasing from 0.64 to 1.17 (Figure A6 a-c). For the AOD-$PM_{10\text{-}2.5}$ relationship, the highest correlation coefficients and slopes were observed under middle PBLH conditions (Figure A6 d-f), underscoring differences between AOD-$PM_{2.5}$ and AOD-$PM_{10\text{-}2.5}$ relationships. In general, deeper PBLH is associated with stronger AOD-PM correlations and greater AOD sensitivity to PM.

The effects of RH on AOD-PM relationships could be manipulated by aerosol humidification, and the RH's effect on cloud. Fig. 12 shows that during the daytime, the slope of the AOD-$PM_{2.5}$ relationship increases with RH, from 0.70 under low RH to 0.81 under moderate RH, and 1.16 under high RH. This can be explained by the fact that higher RH promotes hygroscopic particle growth, leading to increased aerosol extinction and a sharper rise in AOD. The correlation is highest under dry conditions (0.695), followed by high RH (0.627), and lowest under moderate RH (0.583). This pattern suggests that under dry conditions (low RH), most particles do not undergo hygroscopic growth, while

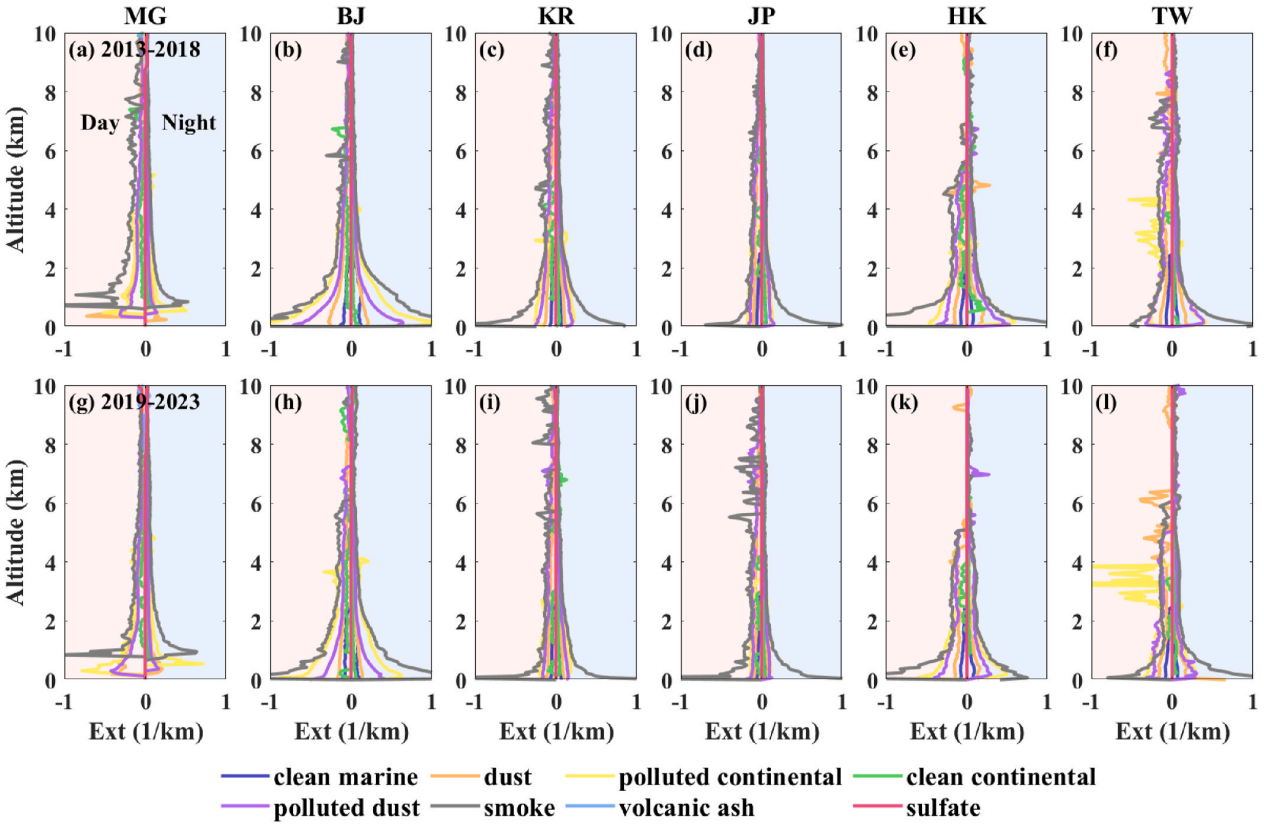

Fig. 6. Averaged extinction profiles of seven aerosol types for the two periods: 2013–2018 and 2019–2023, across the regions MG (a and g), BJ (b and h), KR (c and i), JP (d and j), HK (e and k), and TW (f and l).

under humid conditions (high RH), nearly all particles experience such growth. These two scenarios result in more uniform hygroscopic behavior across particles, leading to stronger AOD-$PM_{2.5}$ correlations. In contrast, under moderate RH, only part of particles undergo hygroscopic growth, which is influenced by aerosol types, leading to heterogeneous growth and lower correlations, as found by Day and Malm (2001). In addition to hygroscopic growth caused by high RH, the high RH also associated with high cloud cover, which in turn increase the AOT via cloud processing, new particle formation, and air convergence (Eck et al., 2018). At nighttime, the slope trends are similar to those observed during the day. However, the correlations under low, moderate, and high RH do not show significant statistical differences, particularly between low and moderate RH. This may be due to more complex aerosol types and finer particle sizes at night, as low PBLH confines aerosols closer to the surface and favors the deposition of coarse particles. The AOD-$PM_{10\text{-}2.5}$ relationship shows a significant increase in correlation under low and high RH compared to the overall cases, observed for both daytime and nighttime. Notably, the highest correlation occurs under high RH at nighttime (0.351), followed by dry conditions at nighttime (0.303), representing increases of approximately 150 % and 113 % compared to the overall correlation (0.142). These values are also the highest among all classified groups (Table A1). Slopes for AOD-$PM_{10\text{-}2.5}$ generally increase with RH, except for a minor difference between low (0.18) and moderate (0.16) RH, which is negligible compared to the slope of 0.82 under high RH. Similarly, the slopes at high RH (0.61 for daytime and 0.82 for nighttime) are three to four times higher than those at low (0.21/0.18) and moderate RH (0.26/0.16) (Table A2). These findings highlight that RH has the strongest impact on the AOD-$PM_{10\text{-}2.5}$ relationship.

The classified groups by temperature generate higher AOD-$PM_{2.5}$ correlations for both daytime and nighttime (Fig. 13). Compared to the overall cases, the grouped AOD-$PM_{2.5}$ correlations are significantly improved across all Temp levels, exhibiting correlation coefficients of 0.723, 0.719, and 0.664 in the daytime, representing increases of 15 %, 14 %, and 5 %, respectively, and 0.687, 0.634, and 0.651 at nighttime, showing increases of 10 %, 2 %, and 5 %, respectively. This improvement is the most pronounced across all categorized groups (Table A1), suggesting that Temp has the strongest influence on AOD-$PM_{2.5}$ relationship. This also suggests that temperature could be the primary meteorological factor that drives the seasonal variations on AOD-$PM_{2.5}$ relationship. It is worth noting that the difference in correlation between low and middle Temp conditions during daytime is minimal, as is the difference between middle and high Temp conditions at nighttime. This suggests that correlations tend to be higher under lower Temp conditions, a trend observed for both daytime and nighttime. The slope is highest under high Temp conditions for both daytime (1.14) and nighttime (1.05), representing increases of 58 % and 78 %, respectively, compared to the lowest slope under middle Temp conditions (0.72 and 0.59) (Table A2). This is mainly because that the increase in temperature could lead to the increases of upward movement of pollutants, thus higher AOD (Tariq and Khan, 2024). To test whether thresholds affect these patterns, Temp was classified into more detailed levels. Similar trends were observed, even with finer Temp classifications, demonstrating the robustness of the analysis with only three Temp levels (Fig. A7). However, the correlation coefficients for the AOD-$PM_{10\text{-}2.5}$ relationship do not show significant improvement under grouped Temp conditions and even decrease at nighttime. Note that all the correlation coefficients and slopes under various categorized groups have been compiled in Table A1 and Table A2, respectively, for the above three meteorological factors.

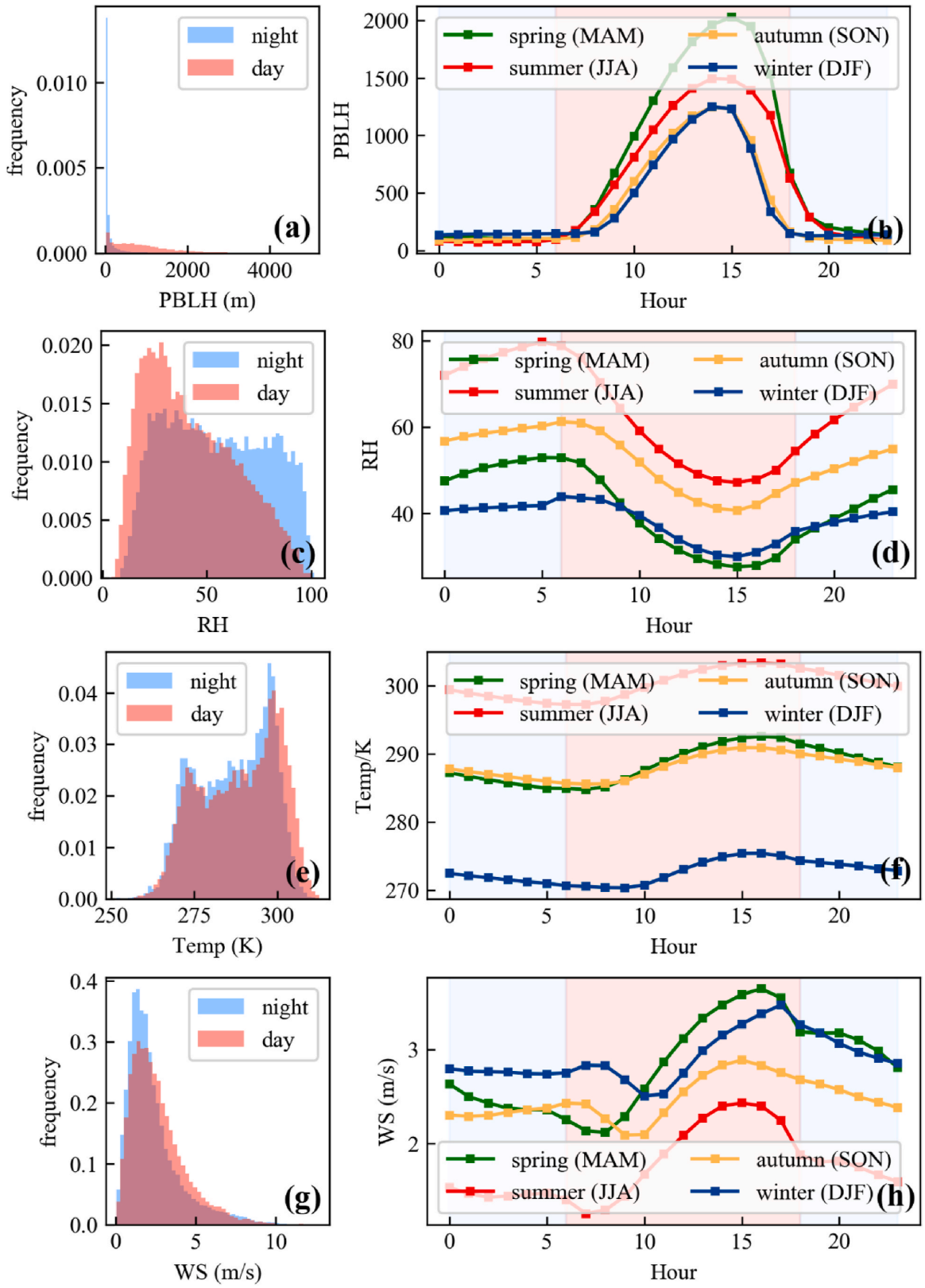

Fig. 7. The histogram distribution of daytime and nighttime RH, PBLH, Temp, and WS and their seasonal, diurnal variations in the selected region of BJ.

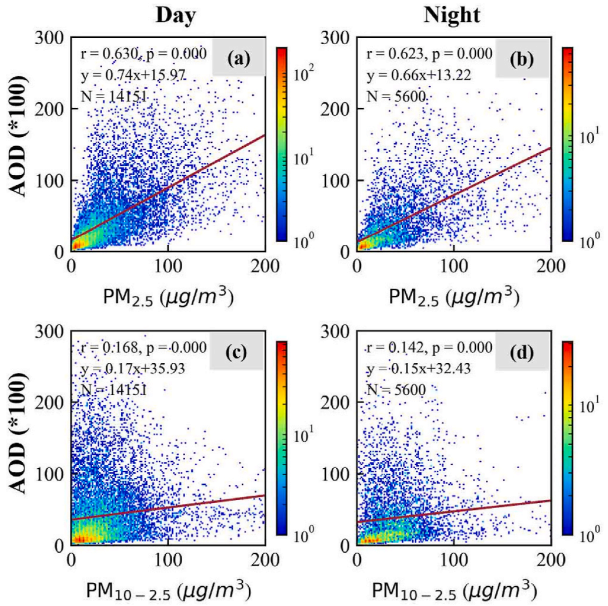

Fig. 8. Scatterplots between AOD (*100) with $PM_{2.5}$/$PM_{10\text{-}2.5}$ at daytime (A/C) and nighttime (B/D).

The wind effect was analyzed only for the relationship between AOD and $PM_{2.5}$, while the correlations between AOD and $PM_{10\text{-}2.5}$ were wot analyzed as they are insignificant under various wind conditions. Both wind direction and wind speed were considered. The seasonal Windrose map at daytime (Fig. A8) show that south is the most frequent direction in BJ during spring, summer and autumn, while northwest is the prevalent one in winter. The two directions account for more than 90 %. In contrast, the nighttime seasonal Windrose map (Fig. A9) indicates that the northwest and north winds are dominant throughout the year in BJ. To simplify the analysis, two major wind directions were explored: north (0°–90° and 270°–360°) and south (90°–270°). Fig. 14 illustrates significant differences in the correlation coefficients for these two directions during both day and night. At daytime, the correlation coefficient for the north direction (0.686) is 18 % higher than for the south direction (0.581). At nighttime, the difference is even more pronounced, with the correlation coefficient for the north direction (0.647) being 26 % higher than for the south direction (0.512). Besides, the regression lines at north direction show slightly higher slopes (0.81/0.69) than at the south direction (0.76/0.57) for both daytime and nighttime. Fig. 15 illustrates how the correlation coefficient varies with WS. The correlation exhibits a nonlinear trend with WS: under low wind speed conditions (WS < 2 m/s), the correlation remains consistently around 0.6. For moderate wind speeds (WS 2–5 m/s), the correlation coefficient increases with increasing wind speed. However, when WS exceeds 5 m/s, the correlation decreases. At nighttime, the correlation trends for different wind directions are generally similar but differ in magnitude and turning points. For the north direction, the correlation coefficient shows a positive trend with WS under low wind speed conditions (0–2 m/s) but decreases sharply under moderate wind speed conditions (2–6 m/s). Beyond 6 m/s, the correlation coefficient increases again as WS increases. In contrast, for the south direction, the turning points occur at lower wind speed thresholds: 1 m/s and 4 m/s for low-to-moderate and moderate-to-high wind speed conditions, respectively.

It could be concluded that the effects of meteorological factors on the AOD-PM relationship are generally consistent. For both daytime and nighttime, high correlation coefficients are typically observed under conditions of high PBLH, low/high RH and low Temp. Additionally, high regression slopes are commonly associated with high PBLH, high RH, and high Temp. However, there is a noticeable discrepancy between day

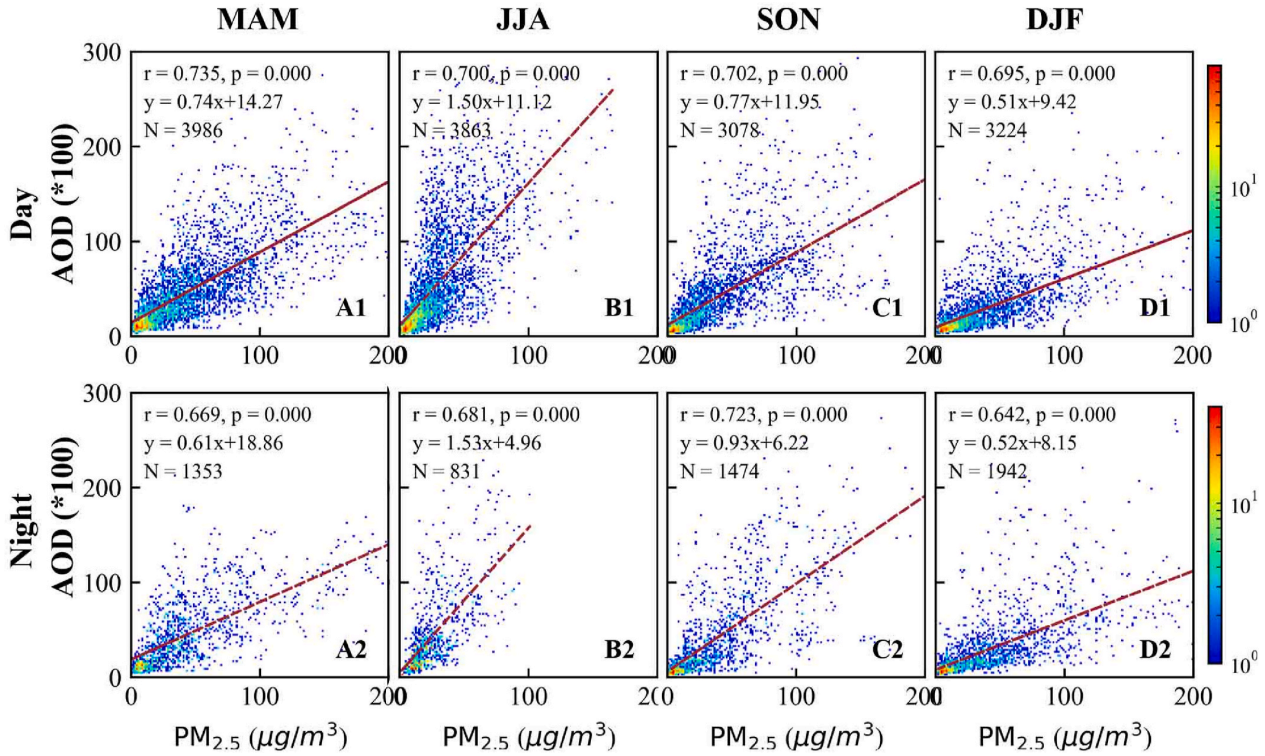

Fig. 9. Seasonal scatterplots between AOD (*100) with PM2.5 at daytime (A1 to D1) and nighttime (A2 to D2).

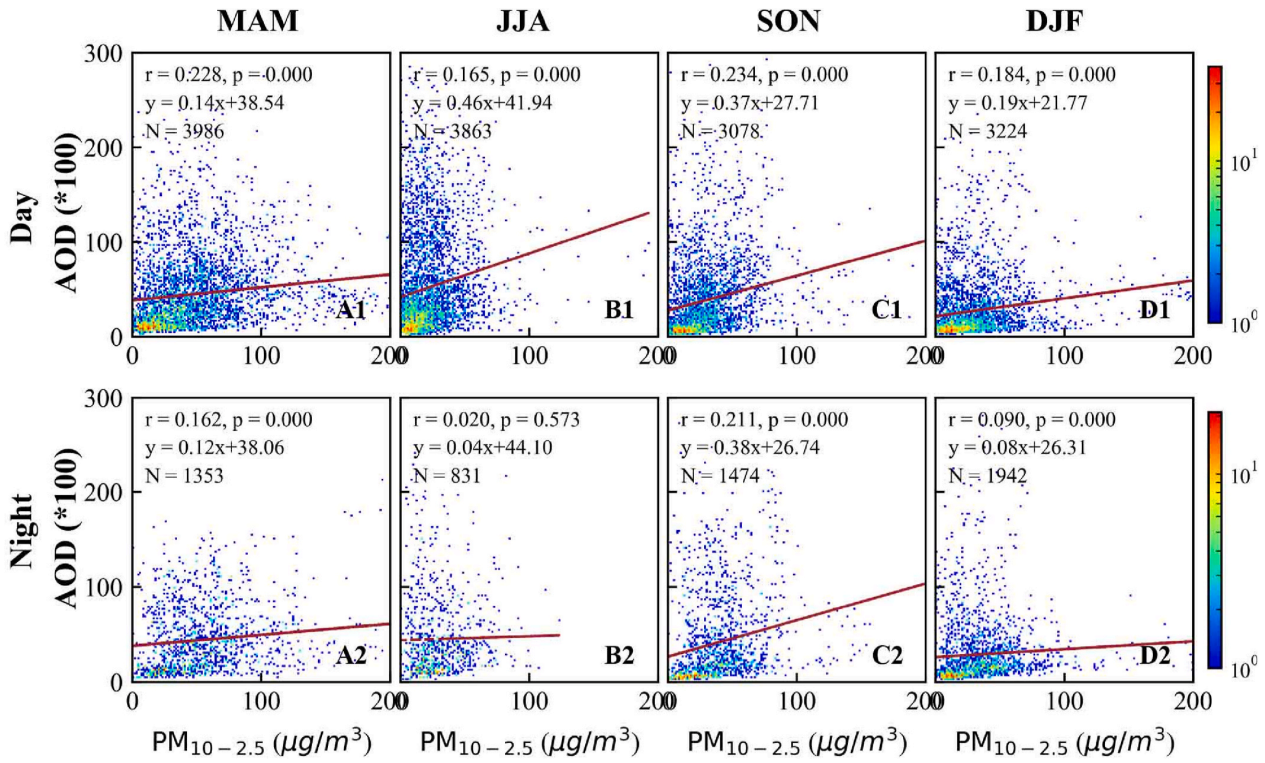

Fig. 10. Seasonal scatterplots between AOD (*100) with $PM_{10\text{-}2.5}$ at daytime (A1 to D1) and nighttime (A2 to D2).

and night. While high correlations are found under both low and high RH during the daytime, high correlations occur only under high RH, with low RH resulting in lower correlations at nighttime.

Notably, meteorological factors may also be interrelated. To investigate whether the effect of one meteorological factor could be influenced by another, the relationships between pairs of meteorological factors were analyzed. Fig. 16 illustrates these relationships. While all relationships were found to be statistically significant with p-value less than 0.001, the correlation coefficients were relatively low, except for two cases: (1) PBLH shows a noticeable negative relationship with RH during the daytime, with a correlation coefficient of 0.620, which has also been found in Zheng et al. (2017), and (2) Temp exhibits a positive correlation with RH at nighttime, with a correlation coefficient of 0.448. During the daytime, the highest correlation coefficient for AOD-$PM_{2.5}$ was observed under conditions of low RH and high PBLH (along with low Temp). To examine whether and how RH influences the effect of PBLH on the AOD-$PM_{2.5}$ relationship during the daytime, further analysis was conducted by constraining PBLH to high levels (PBLH >200 m to ensure sufficient sample size) and categorizing RH into low, middle, and high groups. As shown in Fig. A10(a)–(c), the correlation coefficients (0.719, 0.606, and 0.632) are slightly higher than those in the original categorized RH groups (0.695, 0.583, and 0.627), though these differences are not statistically significant. This indicates that, during the daytime, the effect of high PBLH on the AOD-$PM_{2.5}$ relationship is likely influenced by RH, and the independent effect of PBLH is marginal. At nighttime, high regression slopes were observed under conditions of high RH, high Temp, and high PBLH. To investigate whether and how RH influences the effect of Temp on the AOD-$PM_{2.5}$ relationship at nighttime, further analysis was conducted by constraining Temp to high levels and categorizing RH into low, middle, and high groups. Fig. A10 (d)–(f) reveal that the regression slopes (0.70, 1.16, and 1.32) are considerably higher compared to those in the original categorized RH groups (0.47, 0.65, and 1.01). This suggests that although high Temp is partially associated with high RH, high Temp itself plays a critical role in enhancing the sensitivity of AOD to $PM_{2.5}$. Therefore, Temp could be the most significant contributor to the seasonal dependence of AOD-PM relationship.

5. Discussion

To elaborate on nighttime aerosol characteristics and the differences between daytime and nighttime, this study provides insights from various perspectives including aerosol optical properties across the entire atmospheric column, the vertically decomposed extinction profile, vertically distributed aerosol types, and the influence of meteorological factors on the relationship between AOD and PM. The findings reveal regional variations in day-night differences for columnar aerosol optical properties and vertical extinction profiles, while the vertical distribution of aerosol types remains largely consistent between day and night. Additionally, the influence of meteorological factors on the AOD-PM relationship offers valuable insights into AOD-PM modeling and the prediction of surface PM concentrations. Several other issues relating to our results are discussed below.

5.1. Comparison to existing literatures

The day-night differences in AOD and extinction profiles are mainly influenced by local emissions and meteorological factors, particularly relative humidity (RH). In polluted areas with high local emissions, nighttime AOD and extinction profiles are generally lower than their daytime counterparts. Conversely, in areas with lower local emissions, nighttime AOD and extinction profiles tend to be equivalent to those during the daytime. This can be attributed to lower nighttime temperatures, which lead to increased relative humidity and, consequently, an increase in AOT (Day and Malm, 2001; Jiang et al., 2024). This phenomenon is evident when comparing Fig. A11 (Jiang et al., 2024) with

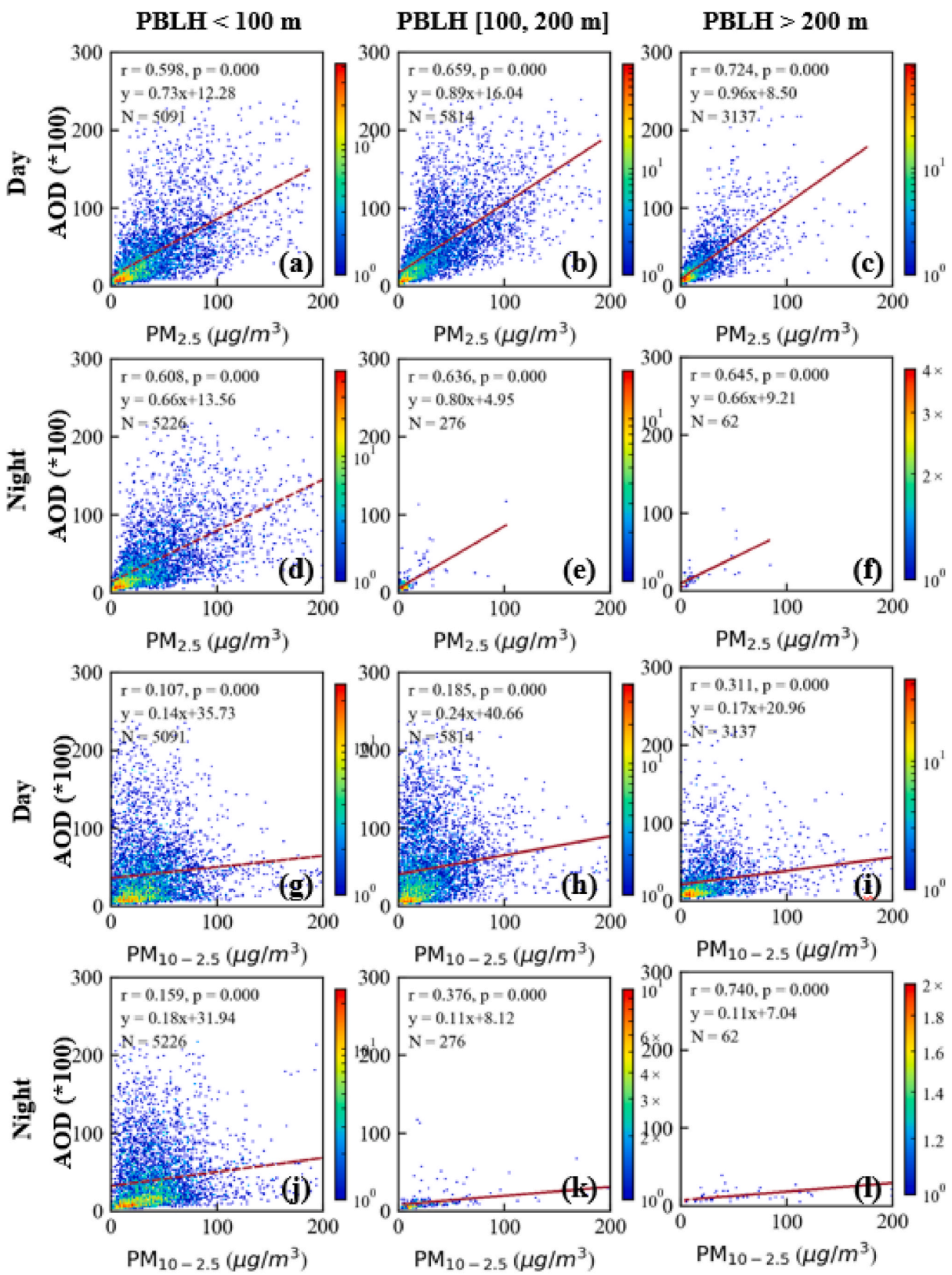

Fig. 11. Scatterplots between AOD and $PM_{2.5}/PM_{10\text{-}2.5}$ under low (PBLH <500 m), middle (500 m < PBLH <1500 m), and high PBLH (PBLH >1500 m) levels at both daytime and nighttime.

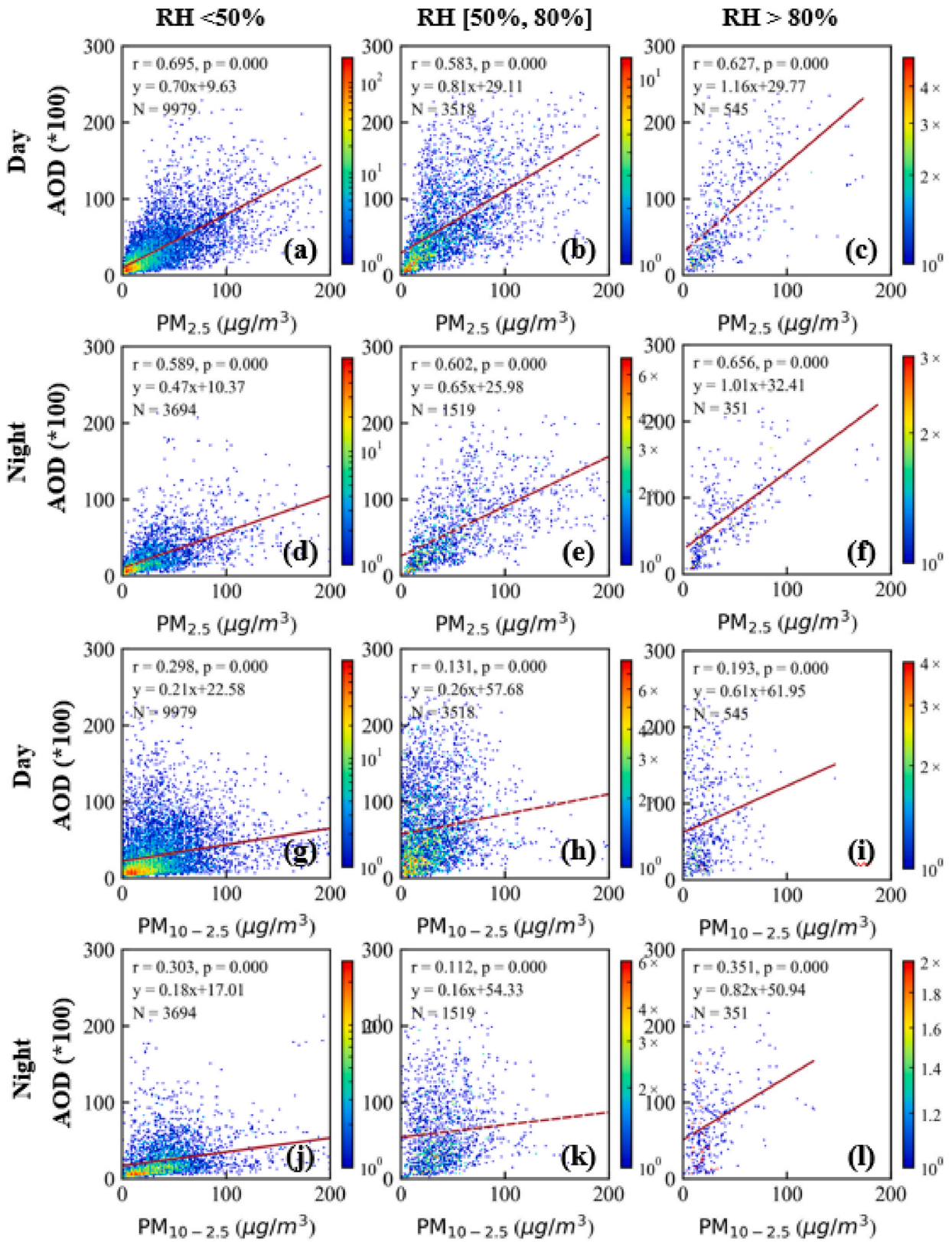

Fig. 12. Scatterplots between AOD and $PM_{2.5}/PM_{10\text{-}2.5}$ under low (RH < 50 %), middle (50 % ≤ RH ≤ 80 %), and high RH (RH > 80 %) levels at both daytime and nighttime.

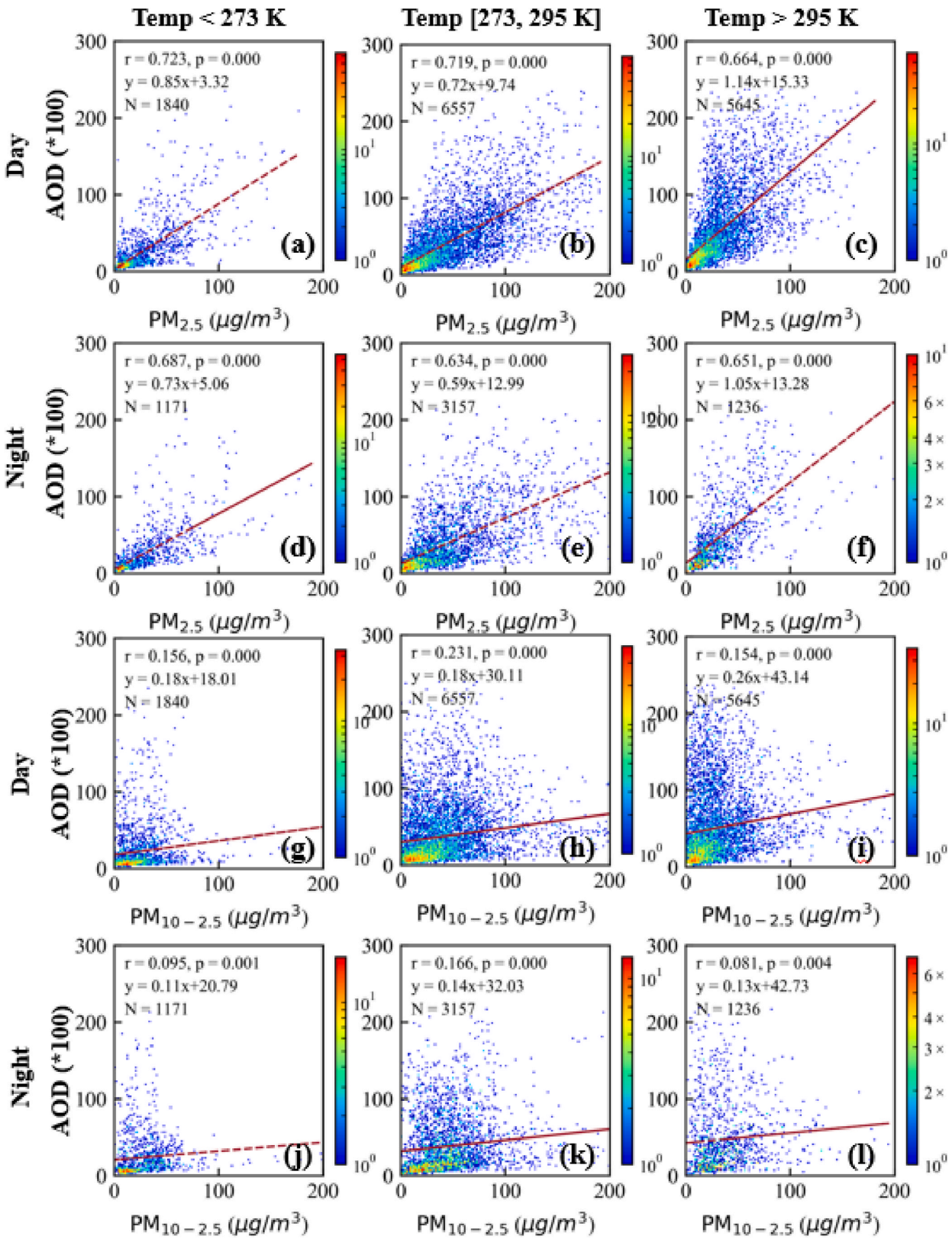

Fig. 13. Scatterplots between AOD and $PM_{2.5}/PM_{10\text{-}2.5}$ under low (Temp <273 K), middle (273 K ≤ Temp ≤ 295 K), and high Temp (Temp >295 K) levels at both daytime and nighttime.

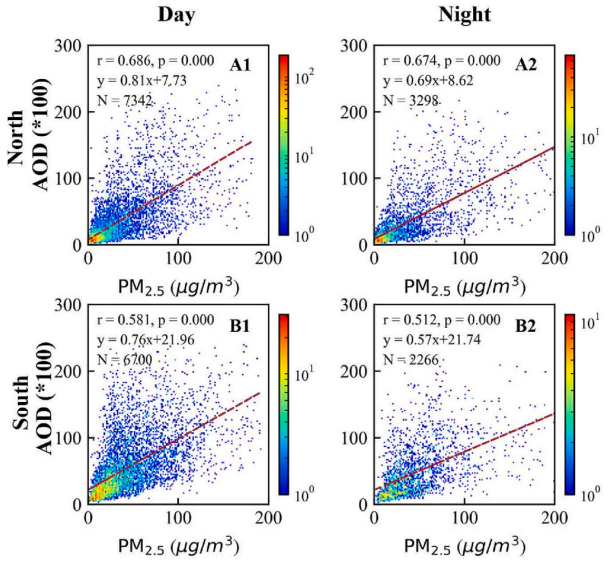

Fig. 14. Scatterplots between AOD and $PM_{2.5}$ at the direction of north and south and under day and night.

Fig. A12 (Wei et al., 2021). The negative values of (Nighttime-Daytime)/Daytime in Fig. A11 (Jiang et al., 2024) align well with the areas exhibiting high $PM_{2.5}$, as shown in Fig. A12 (Wei et al., 2021). Specifically, negative values appear in areas such as the north China Plain (NCP) and Sichuan Basin, which correspond to the areas with high air pollution, whereas positive values are observed in less polluted areas. In this study, we found that nighttime extinction profiles were lower than daytime profiles in Mongolia (MG) for both the 2013–2018 and 2019–2023 periods and in Beijing (BJ) during the 2013–2018 period. However, in BJ, nighttime extinction becomes comparable to daytime extinction from 2019 to 2023. This shift is likely due to improved air quality in the NCP, as evidenced by the spatial distribution of $PM_{2.5}$ from 2000 to 2022 (Wei et al., 2023).

5.2. Rationale of using correlation coefficients and regression slopes

This study employed correlation coefficients and regression slope to analyze the effects of meteorological factors on the AOD-PM relationship. Zheng et al. (2017) have developed the $PM_{2.5}$/AOD ratio to assess the influence of meteorological factors. A smaller ratio indicates stronger aerosol extinction capability. However, this ratio only explains the proportion of surface $PM_{2.5}$ contributing to total aerosol extinction and does not clarify the magnitude of each meteorological factor's effect on the correlation, which is critical for constructing AOD-PM models. Instead of calculating the $PM_{2.5}$/AOD ratio for individual samples, this study used the regression slope derived from all samples to represent the general dependency of AOD on surface $PM_{2.5}$, as it is less affected by outliers. The regression slope analysis revealed that higher PBLH and RH are associated with higher AOD-$PM_{2.5}$ regression slopes, indicating a lower $PM_{2.5}$/AOD ratio. This finding is consistent with Zheng et al. (2017). Our study further revealed that high Temp also leads to high regression slope, and the Temp has a more substantial effect than both the PBLH and RH. Moreover, by analyzing correlation coefficients across various meteorological groups, it was observed that Temp exerts the most significant effect on the AOD-$PM_{2.5}$ relationship, followed by RH and PBLH. In contrast, for the AOD-$PM_{10\text{-}2.5}$ relationship, RH and PBLH have a greater influence than Temp.

5.3. The PBLH effect on AOD-$PM_{2.5}$

Previous studies have indicated that high PBLH reduces the relative contribution of surface PM2.5 to the columnar AOD, primarily due to enhanced vertical transport and mixing of particles (Qu et al., 2016; Zheng et al., 2017). Consequently, one would anticipate a wearer correlation between AOD and surface-level $PM_{2.5}$ under high PBLH conditions. Conversely, a higher correlation is expected under low PBLH, as aerosols tend to be confined closer to the surface. This expectation aligns with the observations in section 4.2, where nighttime aerosol extinction profiles concentrate at low altitudes and rarely exhibit abnormal peaks at higher altitudes. However, the meteorological factor analysis conducted in this study revealed a counterintuitive finding that high PBLH is associated with a strong AOD-$PM_{2.5}$ correlation, as well as a strong AOD-$PM_{10\text{-}2.5}$ correlation. This is contrary to the general understanding.

Further investigation suggests that the effect of PBLH on the AOD-PM relationship could possibly be mediated through its influence on RH. PBLH and RH are inversely related, i.e., high PBLH is generally associated with low RH. That is, high PBLH could lead to low RH, which thus increases the AOD-PM correlation. Additionally, PBLH has a marginal effect on the correlation. This may be caused by the placement of AERONET sites, which are often located on building rooftops to ensure unobstructed illumination. For instance, the altitudes of the Beijing-CAMS, Beijing_PKU, and Yanqihu sites are 106.0 m, 53.0 m, and 100.0 m, respectively, potentially missing aerosol loadings below these levels. Higher PBLH promotes stronger vertical convection and more homogeneous mixing, allowing surface aerosols to be lifted to heights that can be more effectively monitored by AERONET photometers. However, this hypothesis should be further validated using ground-based lidar data in conjunction with AERONET photometer observations in future analysis.

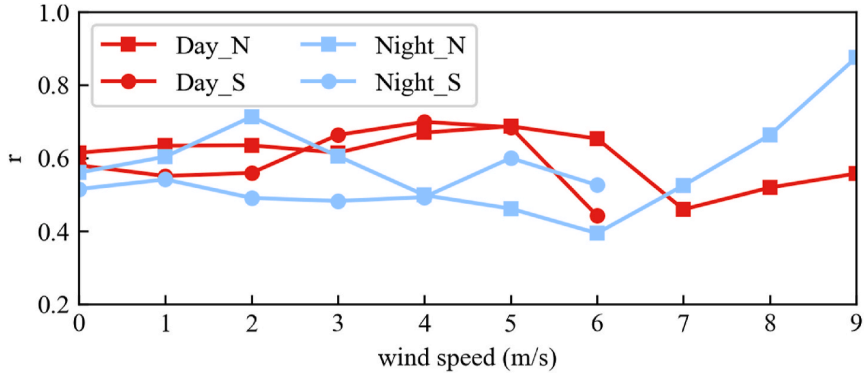

Fig. 15. The correlation coefficient between AOD and $PM_{2.5}$ under varying wind speed levels. The three missing points in the Day_north and Night_north lines are due to the absence of recorded cases by AERONET under high wind speed conditions.

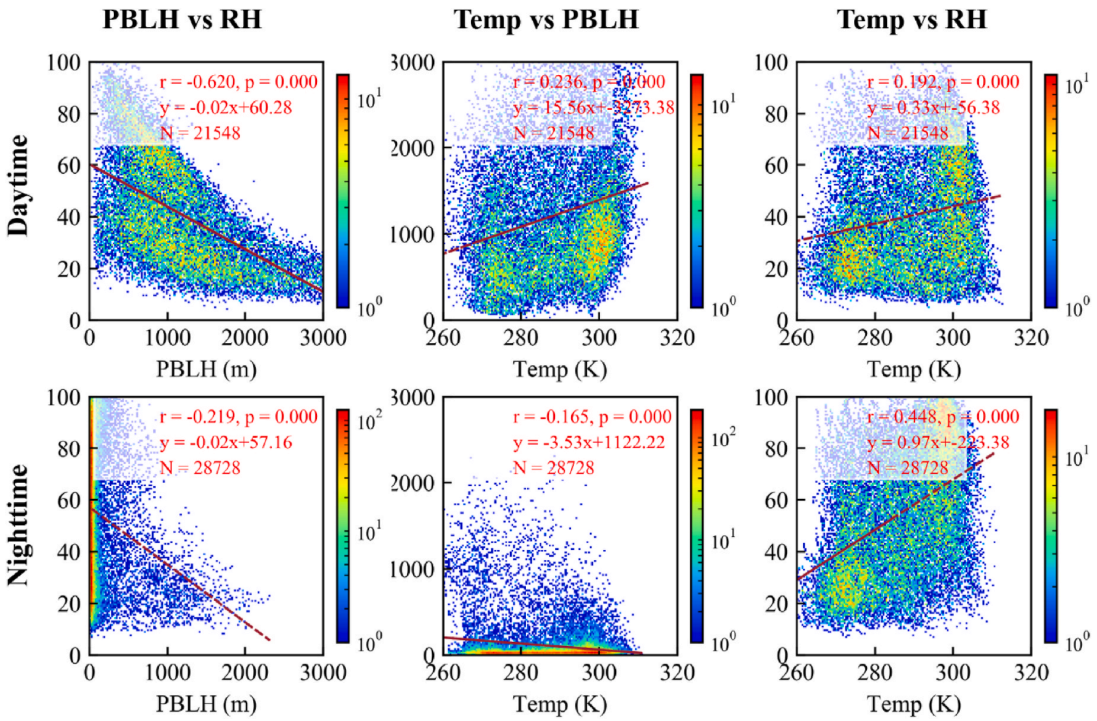

Fig. 16. Scatterplots between two of the meteorological factors.

5.4. The lower correlation coefficient for AOD-PM at nighttime

The vertical extinction profile analysis reveals that the nighttime extinction profiles are concentrated at lower altitudes, as displayed in Section 4.2. This suggests that AOD should have a stronger correlation with near-surface particulate matter during nighttime. However, as shown in Section 4.4, the correlation coefficients at nighttime are similar to or even lower than those during the daytime under various scenarios. This phenomenon could possibly be attributed to the following reasons. Firstly, as illustrated in Fig. 7, nighttime RH predominantly falls within the mid-range (50 %–80 %), leading to heterogeneous hygroscopic growth of aerosol particles. This variability can reduce the correlation between AOD and near-surface particulate matter, as discussed in Section 4.4.3. Secondly, The PBLH at nighttime is significantly lower than during the daytime. As noted in Section 4.4.3, lower PBLH is associated with reduced correlation coefficients, likely due to the confinement of aerosol particles within a smaller vertical range, resulting in less effective mixing. Thirdly, although comparisons of AOD during day-night transition periods show negligible bias between lunar and solar AOD measurements (Schafer et al., 2024), the slightly lower accuracy of the lunar product is mainly due to less effective cloud screening at night, as lunar aureole measurements are unavailable, whereas solar aureole observations are used to detect cirrus clouds during the day.

6. Conclusion

This study integrates ground observations, satellite remote sensing, and model simulation datasets to provide comprehensive and extensive evaluations of nighttime aerosol characteristics in East Asia. It thoroughly investigates the aerosol's optical properties of entire column (AOD and AE), the total and the aerosol-type specific vertical extinction profiles, and the influence of meteorological factors on the relationship between AOD and PM at nighttime, as well as the discrepancies between daytime and nighttime.

The results show that nighttime optical properties, including AOD and AE, are generally consistent with daytime observations. Notably, the northern regions (MG, HK, KR, and JP) exhibit higher day-night consistency compared to the southern regions (TW and HK). Such regional variation is likely influenced by differences in relative humidity (RH) and local emissions. The extremely high RH in TW and HK during summer promotes aerosol hygroscopic growth, resulting in smaller AE values. Besides, the increased AOD in HK at nighttime is likely caused by the increased RH as well as nearby emissions.

Vertical extinction profiles at night are more stable compared to daytime across all six regions. In northern regions, extinction profiles exhibit a sharp exponential decay at lower altitudes and nearly zero extinction at higher altitudes, due to the confined planetary boundary layers. In contrast, TW and HK exhibit secondary extinction peaks at 2–4 km, likely due to transported smoke aerosols. Aerosol-type extinction analyses reveal that smoke aerosols exhibit the highest extinction magnitudes, followed by polluted continental aerosols, polluted dust aerosols, and dust aerosols. In contrast, clean continental and marine aerosols display minimal extinction. The vertical aerosol-type frequency distributions suggest consistent aerosol-type patterns between day and night in all studied regions. Furthermore, the analysis suggests that thin aerosol layers at high altitudes may be undetected by daytime lidar signals but are more effectively captured during nighttime observations.

The influence of meteorological factors on the AOD–PM relationship generally remains consistent between nighttime and daytime, although some discrepancies arise under specific meteorological conditions. Temp notably exerts the strongest influence, significantly contributing to the seasonal dependence observed in the AOD–PM2.5 relationship. Higher planetary boundary layer heights (PBLH) correlate with stronger AOD–PM relationships and increased sensitivity of AOD to PM. Further analysis suggests that the influence of PBLH on the AOD–PM2.5 relationship is likely mediated by RH, considering their strong inverse correlation. RH plays a crucial role in the AOD-PM relationships. Both low and high RH conditions enhance the AOD-$PM_{2.5}$ correlation, though this effect is more pronounced during the daytime than at nighttime. For the

AOD-$PM_{10-2.5}$ relationship, RH has the most substantial impact among the meteorological factors.

This study comprehensively investigates the nighttime aerosol properties in East Asia. The findings enhance our understanding of nighttime aerosols in terms of optical properties, vertical extinction, aerosol type distribution, and the impacts of meteorological factors. These insights can support policymakers in developing strategies to mitigate nighttime aerosol pollution. Furthermore, our findings on the influence of meteorological factors may provide deeper insight and contribute to the quantitative understanding of AOD-PM interactions.

CRediT authorship contribution statement

Jing Li: Writing – original draft, Visualization, Software, Resources, Methodology, Formal analysis, Data curation, Conceptualization. **Jiaqi Jin:** Visualization, Software, Resources, Data curation. **Man Sing Wong:** Writing – review & editing, Supervision, Project administration, Funding acquisition, Conceptualization. **Jun Wang:** Writing – review & editing, Methodology. **Kwon Ho Lee:** Writing – review & editing, Methodology. **Kai Qin:** Writing – review & editing. **P.W. Chan:** Writing – review & editing, Resources.

Declaration of generative AI and AI-assisted technologies in the writing process

During the preparation of this work, the author(s) used ChatGPT in order to assist with revising the manuscript for scientific English. After using this tool/service, the author(s) reviewed and edited the content as needed and take(s) full responsibility for the content of the publication.

Declaration of competing interest

The authors declare the following financial interests/personal relationships which may be considered as potential competing interests: Man Sing Wong reports financial support was provided by Research Grants Council of Hong Kong. If there are other authors, they declare that they have no known competing financial interests or personal relationships that could have appeared to influence the work reported in this paper.

Acknowledgements

This project is substantially funded by the General Research Fund (Grant No. 15603923 and 15609421), and the Collaborative Research Fund (Grant No. C5062–21GF) and Young Collaborative Research Fund (Grant No. C6003–22Y) from the Research Grants Council, Hong Kong, China. The authors acknowledge the funding support (Grant No. BBG2 and CD81) from the Research Institute for Sustainable Urban Development, Research Institute of Land and Space, The Hong Kong Polytechnic University, Kowloon, Hong Kong, China. Jun Wang's participation of work is made possible via in-kind support through the Lichtenberger Family Chair professorship in Chemical Engineering in the University of Iowa. We thank the National Aeronautics and Space Administration (NASA) for providing CALIPSO and AERONET products. Thanks are also given to the European Centre for Medium-Range Weather Forest (ECMWF) for providing ERA5 reanalysis data and the China National Environmental Monitoring Center for offering the $PM_{2.5}$ and PM_{10} data.

Appendix A. Supplementary data

Supplementary data to this article can be found online at https://doi.org/10.1016/j.atmosenv.2025.121388.

Data availability

Data will be made available on request.

References

Ångström, A., 1929. On the atmospheric transmission of sun radiation and on dust in the air. Geogr. Ann. 11 (2), 156–166.
Barreto, A., Cuevas, E., Damiri, B., Guirado, C., Berkoff, T., Berjón, A.J., Hernández, Y., Almansa, F., Gil, M., 2013. A new method for nocturnal aerosol measurements with a lunar photometer prototype. Atmos. Meas. Tech. 6 (3), 585–598.
Charlson, R.J., Schwartz, S.E., Hales, J.M., Cess, R.D., Coakley, J.A., Hansen, J.E., Hofmann, D.J., 1992. Climate forcing by anthropogenic aerosols. Science 255 (5043), 423–430.
Chen, Q., Wang, M., Sun, H., Wang, X., Wang, Y., Li, Y., Zhang, L., Mu, Z., 2018. Enhanced health risks from exposure to environmentally persistent free radicals and the oxidative stress of PM2.5 from Asian dust storms in Erenhot, Zhangbei and Jinan, China. Environ. Int. 121, 260–268.
Chen, Z., Zhou, Z., Ji, C., Yao, Z., Mao, J., Wang, Z., Xiang, Y., Zhang, T., Zhou, Y., Chen, Z., Dou, G., 2025. Comparison of the polluted dust plume and natural dust air mass in a spring dust event in Beijing 2023. J. Environ. Sci. 154, 760–773.
Dagestani, A.A., Tariq, S., Khan, M., Kamal, M., Rehman, M.u., 2024. Assessment of nighttime air quality over an urban location in indo-gangetic Plain using remote sensing observations. Atmos. Pollut. Res. 15 (2), 101982.
Day, D.E., Malm, W.C., 2001. Aerosol light scattering measurements as a function of relative humidity: a comparison between measurements made at three different sites. Atmos. Environ. 35 (30), 5169–5176.
Dubovik, O., Smirnov, A., Holben, B.N., King, M.D., Kaufman, Y.J., Eck, T.F., Slutsker, I., 2000. Accuracy assessments of aerosol optical properties retrieved from Aerosol Robotic Network (AERONET) sun and sky radiance measurements. J. Geophys. Res. Atmos. 105 (D8), 9791–9806.
Eck, T.F., Holben, B.N., Reid, J.S., Dubovik, O., Smirnov, A., O'Neill, N.T., Slutsker, I., Kinne, S., 1999. Wavelength dependence of the optical depth of biomass burning, urban, and desert dust aerosols. J. Geophys. Res. Atmos. 104 (D24), 31333–31349.
Eck, T.F., Holben, B.N., Reid, J.S., Xian, P., Giles, D.M., Sinyuk, A., Smirnov, A., Schafer, J.S., Slutsker, I., Kim, J., Koo, J.-H., Choi, M., Kim, K.C., Sano, I., Arola, A., Sayer, A.M., Levy, R.C., Munchak, L.A., O'Neill, N.T., Lyapustin, A., Hsu, N.C., Randles, C.A., Da Silva, A.M., Buchard, V., Govindaraju, R.C., Hyer, E., Crawford, J. H., Wang, P., Xia, X., 2018. Observations of the interaction and transport of fine mode aerosols with cloud and/or fog in Northeast Asia from aerosol robotic network and satellite remote sensing. J. Geophys. Res. Atmos. 123 (10), 5560–5587.
ECMWF, 2024. ERA5 hourly data on pressure levels from 1940 to present. https://cds.climate.copernicus.eu/cdsapp#!/dataset/reanalysis-era5-pressure-levels?tab=overview. (Accessed 26 April 2024).
Giles, D.M., Sinyuk, A., Sorokin, M.G., Schafer, J.S., Smirnov, A., Slutsker, I., Eck, T.F., Holben, B.N., Lewis, J.R., Campbell, J.R., 2019. Advancements in the Aerosol Robotic Network (AERONET) version 3 database–automated near-real-time quality control algorithm with improved cloud screening for sun photometer aerosol optical depth (AOD) measurements. Atmos. Meas. Tech. 12 (1), 169–209.
Gui, L., Tao, M., Wang, Y., Wang, L., Chen, L., Lin, C., Tao, J., Wang, J., Yu, C., 2022. Climatology of aerosol types and their vertical distribution over East Asia based on CALIPSO lidar measurements. Int. J. Climatol. 42 (11), 6042–6054.
Guo, J., Xia, F., Zhang, Y., Liu, H., Li, J., Lou, M., He, J., Yan, Y., Wang, F., Min, M., Zhai, P., 2017. Impact of diurnal variability and meteorological factors on the PM2.5 - AOD relationship: implications for PM2.5 remote sensing. Environ. Pollut. 221, 94–104.
Hawkins, D.L., 1989. Using U statistics to derive the asymptotic distribution of fisher's Z statistic. Am. Statistician 43 (4), 235–237.
Hersbach, H., Bell, B., Berrisford, P., Biavati, G., Horányi, A., Muñoz Sabater, J., Nicolas, J., Peubey, C., Radu, R., Rozum, I., Schepers, D., Simmons, A., Soci, C., Dee, D., Thépaut, J.-N., 2018. ERA5 Hourly Data on Single Levels from 1959 to Present.
Hien, P.D., Loc, P.D., Dao, N.V., 2011. Air pollution episodes associated with East Asian winter monsoons. Sci. Total Environ. 409 (23), 5063–5068.
Holben, B.N., Eck, T.F., Slutsker, I., Tanre, D., Buis, J., Setzer, A., Vermote, E., Reagan, J., Kaufman, Y., Nakajima, T., 1998. AERONET—A federated instrument network and data archive for aerosol characterization. Rem. Sens. Environ. 66 (1), 1–16.
Hu, Y., Zeng, C., Li, T., Shen, H., 2022. Performance comparison of Fengyun-4A and Himawari-8 in PM2.5 estimation in China. Atmos. Environ. 271, 118898.
Huang, R.-J., Zhang, Y., Bozzetti, C., Ho, K.-F., Cao, J.-J., Han, Y., Daellenbach, K.R., Slowik, J.G., Platt, S.M., Canonaco, F., Zotter, P., Wolf, R., Pieber, S.M., Bruns, E.A., Crippa, M., Ciarelli, G., Piazzalunga, A., Schwikowski, M., Abbaszade, G., Schnelle-Kreis, J., Zimmermann, R., An, Z., Szidat, S., Baltensperger, U., Haddad, I.E., Prévôt, A.S.H., 2014. High secondary aerosol contribution to particulate pollution during haze events in China. Nature 514 (7521), 218–222.
IPCC, 2023. AR6 Synthesis Report: Climate Change 2023. Cambridge University Press, Cambridge, United Kingdom and New York, NY, USA.
Jia, H., Ma, X., Yu, F., Quaas, J., 2021. Significant underestimation of radiative forcing by aerosol–cloud interactions derived from satellite-based methods. Nat. Commun. 12 (1), 3649.
Jiang, X., Wang, Y., Wang, L., Tao, M., Wang, J., Zhou, M., Bai, X., Gui, L., 2024. Characteristics of daytime-and-nighttime AOD differences over China: a perspective from CALIOP satellite observations and GEOS-chem model simulations. J. Geophys. Res. Atmos. 129 (8), e2023JD039158.
Kaufman, Y.J., Tanré, D., Boucher, O., 2002. A satellite view of aerosols in the climate system. Nature 419 (6903), 215–223.
Khan, R., Kumar, K.R., Zhao, T., 2019. The climatology of aerosol optical thickness and radiative effects in Southeast Asia from 18-years of ground-based observations. Environ. Pollut. 254, 113025.

Kittaka, C., Winker, D.M., Vaughan, M.A., Omar, A., Remer, L.A., 2011. Intercomparison of column aerosol optical depths from CALIPSO and MODIS-Aqua. Atmos. Meas. Tech. 4 (2), 131–141.
Koelemeijer, R.B.A., Homan, C.D., Matthijsen, J., 2006. Comparison of spatial and temporal variations of aerosol optical thickness and particulate matter over Europe. Atmos. Environ. 40 (27), 5304–5315.
Köse, A., Tariq, S., Uyal, B.N., Khan, M., Rjoub, H., Mehmood, U., 2024. Analysis of nighttime aerosols and relation to covariates over a highly polluted sub-saharan site using mann–kendall and wavelet coherence approach. J. Environ. Qual. 53 (2), 162–173.
Kumar, A., Hakkim, H., Ghude, S.D., Sinha, V., 2021. Probing wintertime air pollution sources in the indo-gangetic plain through 52 hydrocarbons measured rarely at Delhi & mohali. Sci. Total Environ. 801, 149711.
Li, J., Carlson, B.E., Yung, Y.L., Lv, D., Hansen, J., Penner, J.E., Liao, H., Ramaswamy, V., Kahn, R.A., Zhang, P., Dubovik, O., Ding, A., Lacis, A.A., Zhang, L., Dong, Y., 2022. Scattering and absorbing aerosols in the climate system. Nat. Rev. Earth Environ. 3 (6), 363–379.
Li, J., Wong, M.S., Shi, G., 2024. Multi-faceted analysis of dust storm from satellite imagery, ground station, and model simulations, a study in China. Atmos. Res. 299, 107195.
Li, S., Joseph, E., Min, Q., 2016. Remote sensing of ground-level PM2.5 combining AOD and backscattering profile. Rem. Sens. Environ. 183, 120–128.
Liu, H., Chan, J.C.L., 2002. An investigation of air-pollutant patterns under sea–land breezes during a severe air-pollution episode in Hong Kong. Atmos. Environ. 36 (4), 591–601.
Ma, X., Bartlett, K., Harmon, K., Yu, F., 2013. Comparison of AOD between CALIPSO and MODIS: significant differences over major dust and biomass burning regions. Atmos. Meas. Tech. 6 (9), 2391–2401.
Ma, Z., Dey, S., Christopher, S., Liu, R., Bi, J., Balyan, P., Liu, Y., 2022. A review of statistical methods used for developing large-scale and long-term PM2.5 models from satellite data. Rem. Sens. Environ. 269, 112827.
Man-Hae, K., Omar, A.H., Tackett, J.L., Vaughan, M.A., Winker, D.M., Trepte, C.R., Hu, Y., Liu, Z., Poole, L.R., Pitts, M.C., 2018. The CALIPSO version 4 automated aerosol classification and lidar ratio selection algorithm. Atmos. Meas. Tech. 11 (11), 6107.
Meng, X., Liu, C., Zhang, L., Wang, W., Stowell, J., Kan, H., Liu, Y., 2021. Estimating PM2.5 concentrations in Northeastern China with full spatiotemporal coverage, 2005–2016. Rem. Sens. Environ. 253, 112203.
Peng, K., Xin, J., Zhu, X., Wang, X., Cao, X., Ma, Y., Ren, X., Zhao, D., Cao, J., Wang, Z., 2023. Machine learning model to accurately estimate the planetary boundary layer height of Beijing urban area with ERA5 data. Atmos. Res. 293, 106925.
Qu, W., Wang, J., Zhang, X., Sheng, L., Wang, W., 2016. Opposite seasonality of the aerosol optical depth and the surface particulate matter concentration over the North China plain. Atmos. Environ. 127, 90–99.
Schafer, J., Slutsker, I., Gupta, P., Eck, T.F., Smirnov, A., Lind, E.S., Siniuk, A., Sorokin, M.G., 2024. A11Q-1876. An Update on the AERONET Lunar AOD Product. American Geophysical Union Fall Meeting, Washington DC.
Song, Z., Chen, B., Huang, J., 2022. Combining Himawari-8 AOD and deep forest model to obtain city-level distribution of PM2.5 in China. Environ. Pollut. 297, 118826.
Su, B., Li, H., Zhang, M., Bilal, M., Wang, M., Atique, L., Zhang, Z., Zhang, C., Han, G., Qiu, Z., Ali, M.A., 2020. Optical and physical characteristics of aerosol vertical layers over northeastern China. Atmosphere 11 (5). https://doi.org/10.3390/atmos11050501.
Su, T., Li, Z., Kahn, R., 2018. Relationships between the planetary boundary layer height and surface pollutants derived from lidar observations over China: regional pattern and influencing factors. Atmos. Chem. Phys. 18 (21), 15921–15935.
Tao, M., Chen, L., Wang, J., Wang, L., Wang, W., Lin, C., Gui, L., Wang, L., Yu, C., Wang, Y., 2022. Characterization of dust activation and their prevailing transport over East Asia based on multi-satellite observations. Atmos. Res. 265, 105886.
Tariq, S., Khan, M., 2024. An investigation of nighttime variability in air quality of Naples (Italy) using wavelet coherence. Air Qual. Atmos. Health 17 (2), 231–243.
Tariq, S., Qayyum, F., Ul-Haq, Z., Mehmood, U., 2023. Remote sensing of nighttime air quality over the megacity of Lahore, Pakistan. Urban Clim. 49, 101498.
Wei, J., Li, Z., Cribb, M., Huang, W., Xue, W., Sun, L., Guo, J., Peng, Y., Li, J., Lyapustin, A., Liu, L., Wu, H., Song, Y., 2020. Improved 1km resolution PM2.5 estimates across China using enhanced space–time extremely randomized trees. Atmos. Chem. Phys. 20 (6), 3273–3289.
Wei, J., Li, Z., Lyapustin, A., Sun, L., Peng, Y., Xue, W., Su, T., Cribb, M., 2021. Reconstructing 1-km-resolution high-quality PM2.5 data records from 2000 to 2018 in China: spatiotemporal variations and policy implications. Rem. Sens. Environ. 252, 112136.
Wei, J., Li, Z., Lyapustin, A., Wang, J., Dubovik, O., Schwartz, J., Sun, L., Li, C., Liu, S., Zhu, T., 2023. First close insight into global daily gapless 1 km PM2.5 pollution, variability, and health impact. Nat. Commun. 14 (1), 8349.
Xu, J., Han, F., Li, M., Zhang, Z., Xiaohui, D., Wei, P., 2019. On the opposite seasonality of MODIS AOD and surface PM2.5 over the Northern China plain. Atmos. Environ. 215, 116909.
Yao, F., Wu, J., Li, W., Peng, J., 2019. A spatially structured adaptive two-stage model for retrieving ground-level PM2.5 concentrations from VIIRS AOD in China. ISPRS J. Photogrammetry Remote Sens. 151, 263–276.
Young, S.A., Vaughan, M.A., 2009. The retrieval of profiles of particulate extinction from cloud-aerosol lidar infrared pathfinder satellite observations (CALIPSO) data: algorithm description. J. Atmos. Ocean. Technol. 26 (6), 1105–1119.
Zeng, X., Li, S., Xing, J., Yang, J., Wang, Q., Song, G., Teng, M., Zhou, D., Lu, J., 2023. CALIPSO-observed Southeast Asia biomass-burning influences on aerosol vertical structure in guangdong-hong Kong-Macao greater Bay area. Atmos. Res. 289, 106755.
Zhang, W., Liu, S., Chen, X., Mi, X., Gu, X., Yu, T., 2024. Estimation of all-day aerosol optical depth in the beijing–tianjin–hebei region using ground air quality data. Remote Sens. 16 (8). https://doi.org/10.3390/rs16081410.
Zhang, Y., Sun, K., Gao, Z., Pan, Z., Shook, M.A., Li, D., 2020. Diurnal climatology of planetary boundary layer height over the contiguous United States derived from AMDAR and reanalysis data. J. Geophys. Res. Atmos. 125 (20), e2020JD032803.
Zheng, C., Zhao, C., Zhu, Y., Wang, Y., Shi, X., Wu, X., Chen, T., Wu, F., Qiu, Y., 2017. Analysis of influential factors for the relationship between PM2.5 and AOD in Beijing. Atmos. Chem. Phys. 17 (21), 13473–13489.
Zheng, H., Kong, S., Seo, J., Yan, Y., Cheng, Y., Yao, L., Wang, Y., Zhao, T., Harrison, R. M., 2024. Achievements and challenges in improving air quality in China: analysis of the long-term trends from 2014 to 2022. Environ. Int. 183, 108361.